

NACDEC - IV

Saphira
IIT BOMBAY

Final Design Report

Amal S Sebastian

Goparaju Khushal

Rohit Tembhare

Ronit Shukla

M Vishnu Sankar

Guide: Prof. Dhwanil Shukla

Contents

1	Introduction	3
2	Configuration Analysis and Shortlisting	4
2.1	Configuration convergence	7
2.2	Wing selection	8
2.3	Rotor selection	8
2.4	Final Configuration	9
2.5	Wing position	10
3	Initial Weight Estimation	11
4	Sizing	13
4.1	Methodology	13
4.2	Results	18
5	Rotor blade design	18
5.1	Design Drivers	18
5.2	Design Methodology	19
5.3	Blade Planform for Rotors in tail	23
5.4	Blade Structural Design	24
6	Wing Design	27
6.1	Airfoil Selection	28
6.1.1	Laminar Airfoils	28
6.2	Wing parameters	29
6.3	Wing Structure	31
6.3.1	Wing Structural Design	31
6.3.2	Structural Analysis of the Wing	32
7	Fuselage design	43
7.1	Seating Arrangement and Layout	45
8	Tail Design	48
8.1	Design Considerations	48
8.2	Horizontal And Vertical Tail Volumes	48
9	Final Design	49

10 CFD Simulations for Aircraft	50
10.1 Grid and Mesh Quality	50
10.2 Mesh Metrics	52
10.3 Initial Conditions and Boundary Conditions	53
10.4 Convergence Criteria & Stability	53
10.5 Results	54
11 Mission Profile And Power Requirement	55
11.1 Total Energy Required and Endurance	55
12 Propulsive Units and Power Source	56
12.1 Propulsive Units	56
12.2 Forward Thrust - EDFs	58
12.3 Key Challenges for Power Source	58
12.4 Approach	58
12.5 Final Power Source - Weight and Specifications	63
12.6 Conclusion of Power Calculation	63
13 Weight Distribution	64
13.1 Wing and EDFs	64
13.2 Rotors in the Wing and Empennage	64
13.3 Landing Gear and Avionics	65
13.4 Miscellaneous Weights	65
14 Performance Analysis	66
14.1 Range Study	66
14.2 Forward Flight Analysis	69
14.3 V-n Diagram	70
14.4 Sensitivity Analysis	70
15 Stability Analysis	71
15.1 Longitudinal and Lateral Static Stability.	71
16 Acquisition and Operation Cost Estimation	75
16.1 Operating Cost Estimate	76
17 Conclusion	77

1 Introduction



Figure 1: Final configuration

In response to the Request for Proposal released by The Aeronautical Society of India, we are proud to present our four-seater Electric Vertical Takeoff and Landing aircraft (e-VTOL). The report consists of the entire analysis of our aircraft and design methodology.

Humankind has continuously pushed the frontier of air transportation since the advent of the first flight. Since then the fixed wing aircrafts have undergone game changing technological advancement enabling it to become the most sought passenger carrier vehicle for long distances. On the other hand the vertical take off and landing aircrafts, although took its first flight in 1930, faced numerous technological hurdles and haven't yet established a mode of intercity and intra-city transportation. The advent of battery technology and advancements in digital technology in the last thirty years has increased the possibilities of intra-city and intercity air transportation. 2021 NacDec IV Request for Proposal calls for the design of an eVTOL which can be used for intercity transportation. This RFP draws innovation from potential eVTOLs and several other conceptual eVTOLs that are currently tested and designed respectively. This report outlines the entire work done we have done in attempting to design a VTOL which meets and exceeds the RFP requirements.

2 Configuration Analysis and Shortlisting

The key discussions from the ICR are re-iterated in brevity to the reader to maintain a clarity of our previous work. Based on the critical mission requirement provided in the problem statement we have identified eleven key mission criteria to shortlist the relevant configuration:

Range	Empty weight fraction
Payload	Endurance
Noise	Cruise speed
Max speed	Manufacturability
Safety	Maneuverability
Stability	

We consider two modes of operation cargo and passenger mode in the configuration analysis separately with the goal to see if a common configuration theme arises from the two different approaches.

The Fundamental Scale for Pairwise Comparisons		
Intensity of Importance	Definition	Explanation
1	Equal importance	Two elements contribute equally to the objective
3	Moderate importance	Experience and judgment slightly favor one element over another
5	Strong importance	Experience and judgment strongly favor one element over another
7	Very strong importance	One element is favored very strongly over another; its dominance is demonstrated in practice
9	Extreme importance	The evidence favoring one element over another is of the highest possible order of affirmation

Intensities of 2, 4, 6, and 8 can be used to express intermediate values. Intensities 1.1, 1.2, 1.3, etc. can be used for elements that are very close in importance.

Figure 2: AHP Weights (Source Wikipedia)

Based on the AHP the weights of each of the mission criteria are evaluated in the tables below.

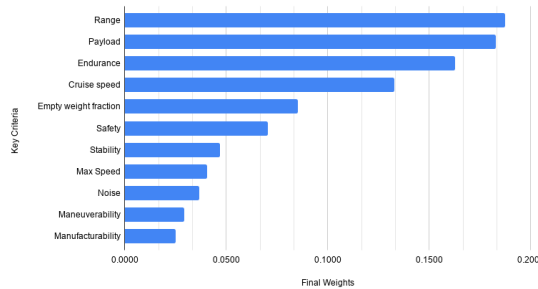
	CARGO											
	Range	Empty weight fraction	Payload	Endurance	Noise	Cruise Speed	Max Speed	Manufacturability	Safety	Maneuverability	Stability	Final Weights
Range	1.00	3.00	2.00	1.00	4.00	2.00	4.00	5.00	4.00	5.00	4.00	0.1875
Empty weight fraction	0.33	1.00	0.25	0.25	3.00	0.20	2.00	3.00	3.00	5.00	3.00	0.0853
Payload	0.50	4.00	1.00	2.00	4.00	3.00	4.00	5.00	3.00	4.00	4.00	0.1826
Endurance	1.00	4.00	0.50	1.00	3.00	2.00	5.00	5.00	4.00	3.00	4.00	0.1626
Noise	0.25	0.33	0.25	0.33	1.00	0.25	0.50	2.00	0.25	2.00	0.50	0.0367
Cruise speed	0.50	5.00	0.33	0.50	4.00	1.00	4.00	5.00	3.00	4.00	3.00	0.1326
Max Speed	0.25	0.50	0.25	0.20	2.00	0.25	1.00	2.00	0.50	1.00	1.00	0.0407
Manufacturability	0.20	0.33	0.20	0.20	0.50	0.20	0.50	1.00	0.33	1.00	0.33	0.0251
Safety	0.25	0.33	0.33	0.25	5.00	0.33	2.00	3.00	1.00	3.00	2.00	0.0705
Maneuverability	0.20	0.20	0.25	0.33	0.25	0.25	1.00	1.00	0.33	1.00	0.50	0.0294
Stability	0.25	0.33	0.25	0.25	2.00	0.33	1.00	3.00	0.50	2.00	1.00	0.0469

(a) AHP for Cargo

	PASSENGER											
	Range	Empty weight fraction	Payload	Endurance	Noise	Cruise Speed	Max Speed	Manufacturability	Safety	Maneuverability	Stability	Final Weights
Range	1.00	3.00	2.00	1.00	4.00	2.00	4.00	5.00	2.00	5.00	3.00	0.2263
Empty weight fraction	0.33	1.00	0.25	0.25	3.00	0.20	2.00	3.00	0.25	4.00	0.33	0.0471
Payload	0.50	4.00	1.00	2.00	4.00	3.00	4.00	5.00	1.00	2.00	1.00	0.0919
Endurance	1.00	4.00	0.50	1.00	3.00	2.00	5.00	5.00	1.00	3.00	1.00	0.1412
Noise	0.25	0.33	0.25	0.33	1.00	0.25	0.50	2.00	0.25	0.50	0.33	0.0389
Cruise speed	0.50	5.00	0.33	0.50	4.00	1.00	4.00	5.00	0.50	3.00	2.00	0.1344
Max Speed	0.25	0.50	0.25	0.20	2.00	0.25	1.00	2.00	0.33	1.00	0.33	0.0389
Manufacturability	0.20	0.33	0.20	0.20	0.50	0.20	0.50	1.00	0.25	0.33	0.25	0.0304
Safety	0.50	4.00	1.00	1.00	4.00	2.00	0.33	4.00	1.00	3.00	2.00	0.1344
Maneuverability	0.20	0.25	0.50	0.33	2.00	0.33	1.00	3.00	0.33	1.00	0.50	0.0410
Stability	0.33	3.00	1.00	1.00	3.00	0.50	3.00	4.00	0.50	2.00	1.00	0.0754

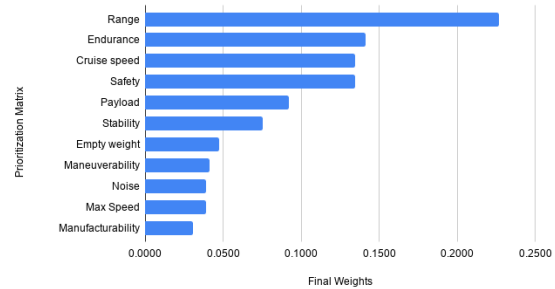
(b) AHP for Pax.

Cargo | Key Criteria and Weights



(c) AHP Weights for Cargo

Pax. | Key Criteria & Weights



(d) AHP weights for Pax.

Figure 3: Weights from Analytical Hierarchy process of Key Criteria

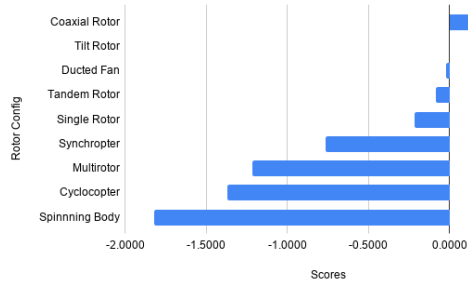
CARGO										
Key criteria	Tilt Rotor	Single Rotor	Coaxial Rotor	Tandem Rotor	Multirotor	Synchropter	Ducted Fan	Cyclocopter	Spinnning Body	
Range	0	-3	-2	-3	-4	-3	0	-2	-2	
Empty weight fraction	0	1	0	1	-2	2	-2	-1	-1	
Payload	0	-1	1	1	-2	1	-1	-3	-2	
Endurance	0	3	2	2	2	1	1	0	-1	
Noise	0	1	0	0	-1	-1	1	1	0	
Cruise speed	0	-2	-1	-1	-2	-3	0	-1	-2	
Max Speed	0	-2	-1	-2	-2	-3	0	-2	-3	
Manufacturability	0	2	1	1	-1	-1	1	-2	-3	
Safety	0	2	1	1	0	-1	1	-1	-2	
Maneuverability	0	1	1	0	2	1	-2	1	-3	
Stability	0	1	2	0	2	-2	2	-2	-3	
Scores	0	-0.2144	0.1784	-0.0877	-1.2165	-0.7635	-0.0232	-1.3708	-1.8209	

(a) Pugh Matrix for Cargo

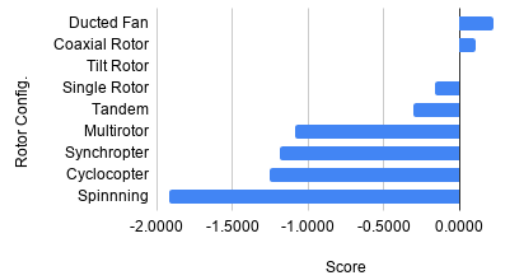
PAX.										
Key Criteria	Tilt Rotor	Single Rotor	Coaxial Rotor	Tandem Rotor	Multirotor	Synchropter	Ducted Fan	Cyclocopter	Spinnning Body	
Range	0	-3	-2	-3	-4	-3	0	-2	-2	
Empty weight fraction	0	1	0	1	-2	2	-2	-1	-1	
Payload	0	-1	1	1	-2	1	-1	-3	-2	
Endurance	0	3	2	2	2	1	1	0	-1	
Noise	0	1	0	0	-1	-1	1	1	0	
Cruise speed	0	-2	-1	-1	-2	-3	0	-1	-2	
Max Speed	0	-2	-1	-2	-2	-3	0	-2	-3	
Manufacturability	0	2	1	1	-1	-1	1	-2	-3	
Safety	0	2	1	1	0	-1	1	-1	-2	
Maneuverability	0	1	1	0	2	1	-2	1	-3	
Stability	0	1	2	0	2	-2	2	-2	-3	
Scores	0	-0.1618	0.1051	-0.3049	-1.0838	-1.1852	0.2277	-1.2538	-1.9197	

(b) Pugh Matrix for Pax.

Rotor Config vs. Scores



Rotor Config vs. Score



(c) Scores for Cargo

(d) Scores for Pax.

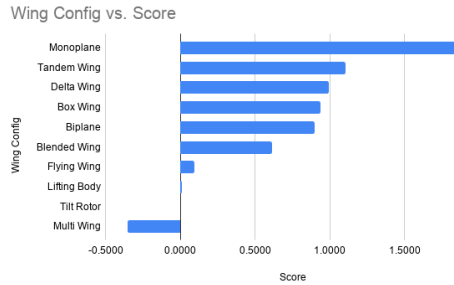
Figure 4: Pugh Matrix for deciding Rotor Configuration

Key criteria	CARGO									
	Tilt Rotor	Monoplane	Biplane	Tandem Wing	Multi Wing	Flying Wing	Blended Wing	Delta Wing	Lifting Body	Box Wing
Range	0	2	1	2	-1	1	1	1	-1	1
Empty weight fraction	0	2	0	0	-1	-1	0	0	0	0
Payload	0	1	1	1	-1	-1	0	-1	-2	1
Endurance	0	3	3	3	3	3	3	3	3	3
Noise	0	1	0	0	-1	1	1	0	-2	1
Cruise speed	0	2	-1	-1	-2	-1	0	3	3	0
Max Speed	0	3	-1	0	-2	-1	0	3	3	1
Manufacturability	0	3	2	0	0	0	-1	1	-2	-1
Safety	0	2	1	1	0	-1	0	0	-2	0
Maneuverability	0	1	0	1	0	-2	-1	0	-3	1
Stability	0	2	2	2	0	-1	-1	-1	-2	0
Scores	0	1.9797	0.8993	1.1066	-0.3509	0.0946	0.6106	0.9909	0.0084	0.9396

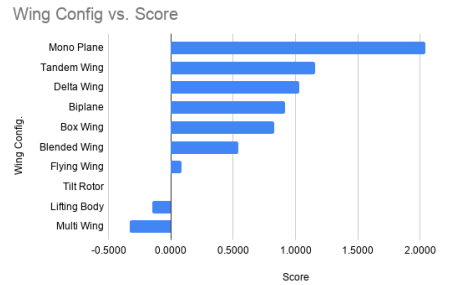
(a) Pugh Matrix for Cargo

Key Criteria	PAX.									
	Tilt Rotor	Mono Plane	Biplane	Tandem Wing	Multi Win	Flying Wing	Blended Wing	Delta Wing	Lifting Body	Box Wing
Range	0	2	1	2	-1	1	1	1	-1	1
Empty weight fraction	0	2	0	0	-1	-1	0	0	0	0
Payload	0	1	1	1	-1	-1	0	-1	-2	1
Endurance	0	3	3	3	3	3	3	3	3	3
Noise	0	1	0	0	-1	1	1	0	-2	1
Cruise speed	0	2	-1	-1	-2	-1	0	3	3	0
Max Speed	0	3	-1	0	-2	-1	0	3	3	1
Manufacturability	0	3	2	0	0	0	-1	1	-2	-1
Safety	0	2	1	1	0	-1	0	0	-2	0
Maneuverability	0	1	0	1	0	-2	-1	0	-3	1
Stability	0	2	2	2	0	-1	-1	-1	-2	0
Scores	0.0000	2.0387	0.9147	1.1602	-0.3271	0.0847	0.5421	1.0330	-0.1478	0.8303

(b) Pugh Matrix for Pax.



(c) Scores for Cargo



(d) Scores for Pax.

Figure 5: Pugh Matrix for deciding Wing Configuration

2.1 Configuration convergence

Following are the top three accepted configurations whose combinations can be taken into further consideration

Coaxial Ducted Fan Tilt rotor	Monoplane Tandem Wing Delta Wing
-------------------------------------	--

Further there are six combinations possible as shown below

		Fuselage Orientation
		Traditional
Platform	Coaxial Rotor	Tandem Wing
		Delta Wing
	EDFs	Monoplane
	EDFs	Tandem Wing
		Delta Wing
		Monoplane

Figure 6: Possible Configurations

2.2 Wing selection

Delta Wings are generally used for high speed aircrafts and for aircraft with mission requirements focusing on maneuverability which is generally the case in combat aircraft, it isn't much suitable for our mission requirements of the eVTOL.

Tandem Wing are generally useful when we want to distribute the lifting loads which is structurally good, but use on tandem wings have more 3D effects and have more induced drag when compare to a monoplane wing producing the same lift.

After comparing with the above wing configurations we decided to go with monoplane as our wing configuration.

2.3 Rotor selection

Electrically Ducted Fans (EDFs) have the highest efficiency in forward flight, but it consumes more power in hovering compared to any rotor system. For EDFs the power consumption is given by

$$P = \sqrt{\frac{\left(\frac{T}{T_i}\right)}{2\rho A}}$$

where $T_i = 1.26$ for ducted fans and T is the weight supposed to be carried by one ducted fan. So for n number of fans (let's say 36 as in the case of Lilium jet) the total power consumption nP which is proportional to $\sqrt{\frac{n}{r}}$ and r is usually small

for EDFs. Whereas for a rotor the ratio $\sqrt{\frac{n}{r}}$ can be easily reduced by increasing the radius and decreasing the number of rotor systems. In short EDFs works best in forward flight and rotor systems works best in hovering and climbing up.

Coaxial rotors have the advantage of providing same thrust with smaller rotor radius compared to a single rotor configuration, and no separate anti torque system is required. But this comes at the cost of added weight, complexity and higher power consumption.

Tilt rotors are not only complex they add enormous weight to the system, they are also inefficient when compared to EDFs due to the high induced losses and improperly streamined flow in the wake of the rotor. To tackle this issue ducted rotors can be used which again comes at the cost of increased mass.

In conclusion the tilt rotor configuration was eliminated due to increased complexity, mass and inefficient power consumption. To optimize the power consumption the best strategy is to incorporate both rotor system and EDFs.

2.4 Final Configuration

Platform	Coaxial Rotor and EDFs	Fuselage Orientation	Wing Position
		Traditional	
		Monoplane	High Wing
			Mid Wing
			Low Wing

Figure 7: Final Configuration

Final configuration consists of a mono-wing, coaxial rotor system used in hover mode and EDFs used in forward flight to optimize the power consumption. The coaxial rotors are embedded inside the wing, closer to the root, so that it is not exposed to air in the forward flight which can cause unnecessary parasite drag. There is also an added advantage that the coaxial system is also in a ducted environment as it is enclosed inside the wing, this reduces induced losses and streamlines the flow. The wing is blended to decrease the interference with the fuselage and also to provide sufficient chord length to enclose the rotors. There are shutters present in the wings which opens during hover phase, closes during forward flight and thus maintains an undisturbed flow over the wing surface during the forward flight.



Figure 8: Retractable Shutters from Pegasus

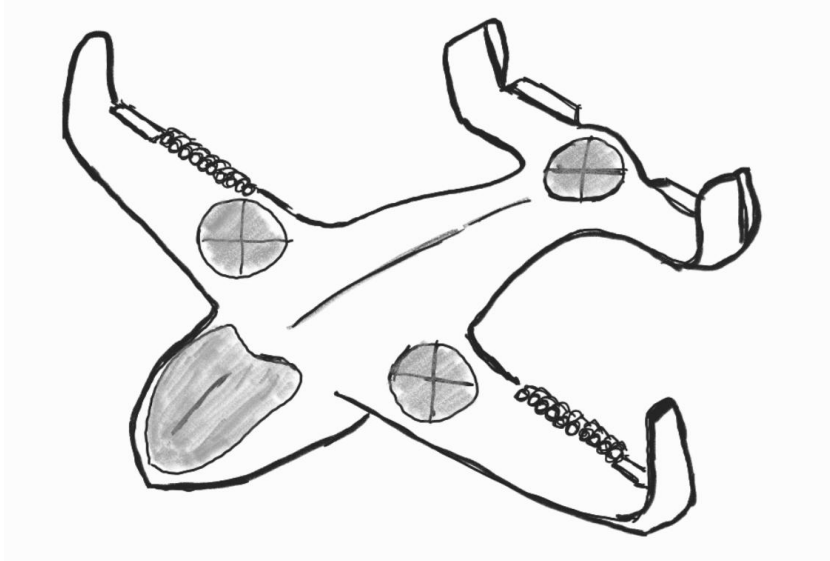


Figure 9: Initial Proposed Configuration

2.5 Wing position

Low Wing

Since the coaxial rotors are installed in the wings, a low wing cannot provide enough space for the downwash to develop as the ground is directly obstructing the flowfield. There also possibilities of unwanted dusts which can get sucked up into the rotor and thus a low wing configuration was ruled out.

Mid Wing

The only issue with the mid wing is the placement of the wing carry box inside the fuselage, this structure placed inside the fuselage can cause inconvenience to passengers and can occupy the space allotted to the cargo, so this possibility was also ruled out.

High Wing

Although high wing has added mass and extra fairings which cause unnecessary drag it gives sufficient ground clearance for the rotor to operate and also rules out the possibility of dusts getting sucked into the rotor. This design requirement is critical to the placement of the coaxial rotors inside the wings, thus this mount position for the wings was preferred over low and mid mount wings.

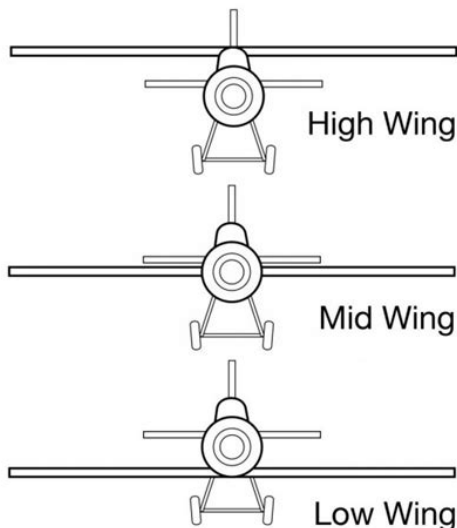


Figure 10: Wing mount

3 Initial Weight Estimation

Before we go ahead and design our eVTOL, we must have some initial numbers to start with. The information we have with us is the constraint of our payload that is 500kgs. From this, we have to find out a crude estimate of the empty weight of our vehicle. There are many ways to land up at appropriate numbers for a start. As there is no well known technique for eVTOLs to find this, we can just take a

	Model	Empty Weight	Payload	MTOW	Payload Fraction
Mentioned in the ICR	Alakai Skai	1575	454	2029	0.224
	Ehang 216	360	220	580	0.38
	Bell Nexus	2800	400	3200	0.125
	S4 Joby	1815	400	2215	0.181
	Lilium 2 seater	440	200	640	0.313
Other designs	S2 Joby	1800	375	2175	0.173
	Ehang 184	250	100	350	0.286
	Uber Elevate eCRM-001/004	1815	444	2259	0.197
	Happy Takeoff Prism	2267	544	2811	0.194
	Pegasus Universal Aerospace				
	Business Jet	5000	700	5700	0.123
	Volocopter VC200	300	150	450	0.334
	aeroG Aviation aG-4 Liberty	4681	907	5588	0.163
	Terrafugia TF-2 Tiltrotor	3500	460	3960	0.117
	UAS-75: Akshat NX	55	20	75	0.267
VTOL Aviation India Designs	UAS-150: Akshat NX	100	50	150	0.334
	UAS-300: Akshansh NX	200	100	300	0.334
	UAS 500: Aaryan NX (Manned)	400	100	500	0.2
	UAS 800: Abhiyaan EUM	600	200	800	0.25
	UAS 800: Abhiyaan NX (Air Taxi)	600	200	800	0.25
	UAS 1800: Kirtiman NX (Air Taxi)	1330	470	1800	0.262

Table 1: Survey of similar VTOL aircrafts for the initial weight estimation.

simpler route, examining the trends of empty weight fraction with payloads. The reason of this being that whatever initial estimate we take, we are going to end up using an iterative process of a sizing algorithm to land up in proper estimates of total weight.

For the purpose of initial weight estimation, we examined an exhaustive list of eVTOLs from the eVTOL database and considered the designs which were close to our deliverables of the problem statement. Table 1 enlists them all. The gross weight and the payload or simply payload fraction and total weight was noted down for many eVTOLs and a trendline was plotted to see the variation of payload fraction with respect to payload.

Figure 11 shows the trend formed by conceptual designs like Lilium Jet, S2 Joby, Alakai S'kai, Uber Elevate and many other eVTOLs, some of them which have also been tested for flight. Through this trendline, we expect that a reasonable

Payload and Payload Fraction

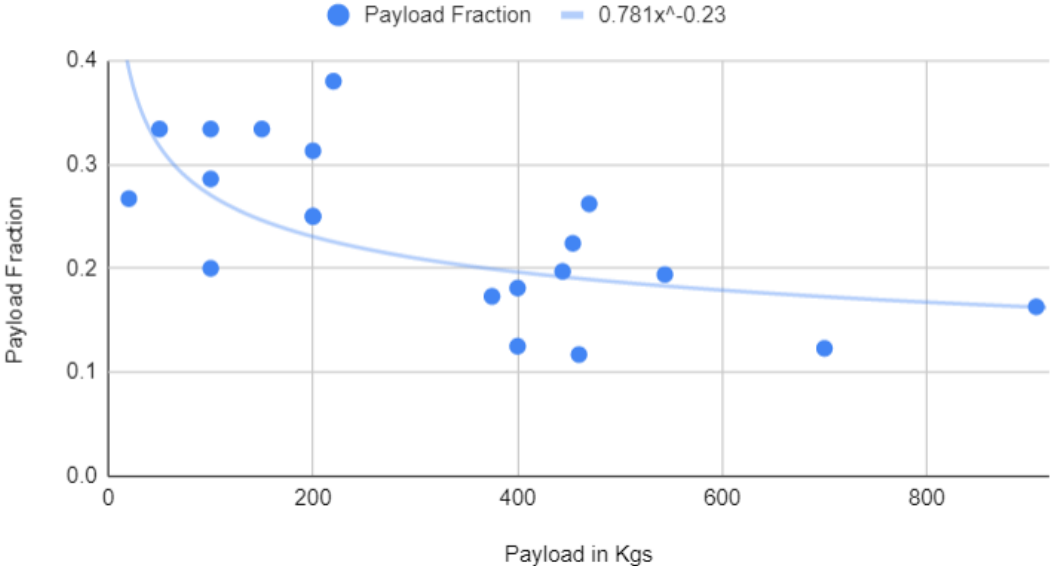


Figure 11: Trendline function for Payload fraction v/s Payload

value for payload fraction will be obtained for our designated 500 kgs of payload. From the trendline function we got a value of 2183 kgs of empty weight which in turn gave us the gross take off weight as 2683 kgs. Hence we now have an initial number to start off our sizing algorithm with and reach a convergence for the gross weight and the parts of the VTOL. Further usage of this value is presented in the next section.

4 Sizing

4.1 Methodology

To carry out the sizing we more or less followed the approach as mentioned in Xiao et al., 2020 [12]. We wrote an in house code to implement a modified version of the proposed algorithm.

Each individual design which was considered was an unique combination of the three variable: aspect ratio (AR), number of EDFs/propellers (N), and the ratio of the wing span swept by the EDFs/propellers (BS).

Parameter	Minimum	Maximum
AR	4.5	15
N	2	20
BS	0.05	0.95

Table 2: Design Space boundaries

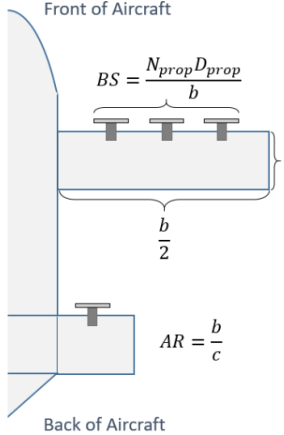


Figure 12: Top view of the vehicle with the design variables being optimized for

Each variable has a minimum and maximum possible value based on a feasible design space boundary, defining a range from which the algorithm can choose design points. Details of the values used by us can be found in table 2.

To aid in the sizing iteration, aircraft designers typically use power loading versus wing loading constraint curves which depict the rated power of the vehicle's power plant and wing surface area are inversely normalized to the aircraft's total weight.

Constraint curves are dependent on the mission profile and vary greatly with each flight phase. Equations 1-5 give the expressions used to calculate constraint curves during cruise and climb.

$$k = \frac{1}{\pi e AR} \quad (1)$$

$$q = \frac{1}{2} \rho v^2 \quad (2)$$

$$(T/W)_{cruise} = \frac{g}{1000} \left(\frac{q C_{D0}}{W/S} + k \frac{W/S}{q} \right) \quad (3)$$

$$(T/W)_{climb} = \frac{g}{1000} \left(\frac{RC}{v} + \frac{qC_{D0}}{W/S} + k \frac{W/S}{q} \right) \quad (4)$$

$$W/S = 0.5 \times \rho v_{stall}^2 C_{L_{max}} \quad (5)$$

$$P/W = \frac{(T/W)v}{\eta_p} \quad (6)$$

where e is the Ostwalds factor, AR is the aspect ratio and η_p is the propulsive efficiency. All other notations are as followed in standard notation.

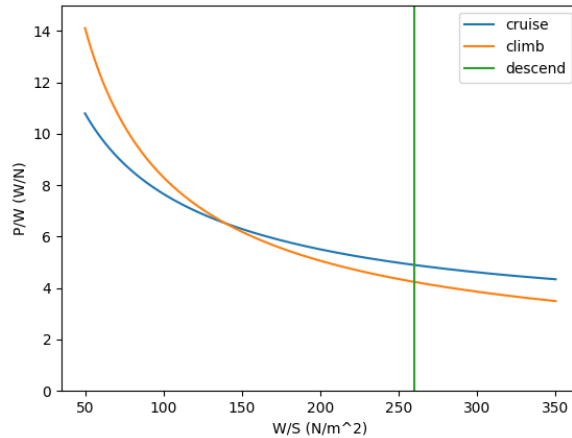


Figure 13: Constraint Analysis

A typical curve generated for a given set of design variables is shown in Figure 13.

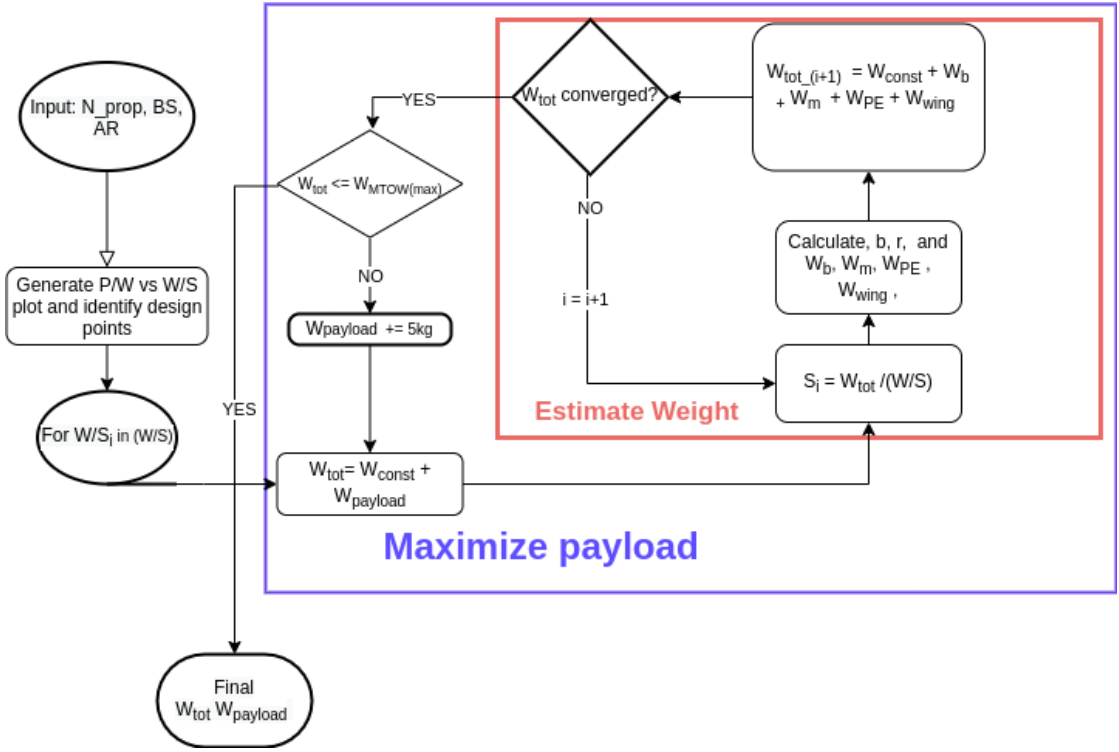


Figure 14: Sizing Process

Once we extract the wing and power loading from the constraint curves by choosing a suitable design point we then proceed to carry out an iterative weight estimation of the various weight components as well as the payload of the plane are shown in Figure 14 (flowchart).

To kick start the iteration, an initial MTOW estimate is made using the sum of W_{const} and the current payload. The current payload starts off as 0 kg but is incremented upon convergence until the desired MTOW is reached.

The following equations were used in the weight estimation loop [5, 12]:

$$S_i = \frac{W_{tot_i}}{(W/S)_j} \quad (7)$$

$$b_i = \sqrt{AR \cdot S_i} \quad (8)$$

$$r_i = \frac{b_i \cdot BS}{2N_{prop}} \quad (9)$$

$$P_{TOL_i} = \frac{N_p}{\eta_p} \sqrt{\frac{(W_{tot_i}g)^3}{2N^3\rho\pi r_i^2}} \quad (10)$$

$$[E_{TO_i}, E_{L_i}] = \frac{[t_{TO}, t_L] P_{TOL_i}}{3600000} \quad (11)$$

$$E_{climb_i} = \frac{W_{tot_i} t_{climb}}{3600(W/P)_{climb_j}} \quad (12)$$

$$E_{cruise_i} = \frac{W_{tot_i} t_{cruise}}{3600(W/P)_{cruise_j}} \quad (13)$$

$$E_{hover} = P_{hover} * t_{hover} \quad (14)$$

$$E_i = E_{TO} + E_L + E_{climb} + E_{cruise} + E_{hover} \quad (15)$$

$$W_{PE_i} = \frac{W_{tot_i}}{\min((W/P)_{climb_j}, (W/P)_{cruise_j}) \cdot SP_{PE}} \quad (16)$$

$$W_{wing_i} = \sigma_{wing} S_i \quad (17)$$

$$W_{M_i} = \frac{W_{tot_i}}{\min((W/P)_{climb_j}, (W/P)_{cruise_j}) \cdot SP_M} \quad (18)$$

$$W_{b_i} = \max\left(\frac{P_{TOL_i}}{SP_b}, \frac{E_i}{SE_b}, \frac{P_{hover}}{SP_b}\right) \quad (19)$$

$$W_{tot_{i+1}} = W_{const} + \Sigma W_i \quad (20)$$

where,

W_{tot_i} - total weight in i^{th} iteration

W_{PE} - Weight of power electronics

W_{wing} - Weight of wing

W_M - Weight of motors

W_b - Weight of battery

Depending on the wing and power loading the iteration will either converge or grow unbounded. We look to find the set of design variables which gives us the best payload.

Parameter	Value
AR	8.0
N	12
BS	0.6
P/W	6.52 W/kg
W/S	139 kg/m ²
W_{total}	3506.792 kg
$W_{payload}$	865 kg
$W_{battery}$	1172.815 kg
W_{wing}	275 kg
b (wing span)	12.302 m
c (average chord length - wing)	1.5 m

Table 3: Sizing results

4.2 Results

Given in Table 3 are the results of the best iteration obtained.

5 Rotor blade design

An in-house Numerical Blade Element Momentum Theory (BEMT) algorithm was developed, along with Prandtl's tip-loss function, in Python to analyze the performance of the rotor system. Although coaxial rotors are used in the final configuration, the in-house algorithm is used to analyze mono-rotors and the power consumption of coaxial rotors is accounted using the approach as discussed in [10]. Since the MTR a few significant modifications have been accounted in the rotor design. Earlier only three pair of co-axial rotors were proposed: Two in the wings and one in the empennage. Due to dimensional constraints and structural constraints from the wing design, we finally propose to have four pair of coaxial rotors which are about only half the size of the rotors which was proposed in MTR. The design of coxials rotors in the empennage remains unchanged and hence the calculations done earlier remain unaltered.

5.1 Design Drivers

Design of the rotors is a three step iterative process, in each process the design drivers based on their relative importance are identified and evaluated first.

1. General Sizing: Primary design drivers are evaluated on the basis of existing data and curve fitting, the detailed approach is explained in sections below.

- (a) Rotor diameter
 - (b) Disk loading
 - (c) Rotor Tip Speed
2. Blade Planform: Secondary design drivers
- (a) Solidity
 - (b) Chord length
 - (c) Number of blades
 - (d) Blade twist

There are several trade-offs in performance and other characteristics that vary with these parameters, also these parameters are interdependent and the optimum value is chosen after a parametric study which will be explained in the Blade Planform section

3. Airfoil Selection

For all the calculations NACA 2421 is considered as the final choice as it has the sufficient thickness to maintain structural integrity and has high stall angle which is necessary for the root section to escape stall. Although different airfoil sections at different radial locations can be installed to optimize the performance with minimum power consumption, such modifications are more efficient only when the rotor length is large. Since the rotor' radius used in the wing is just 62.5 cm, a simple design is proposed.

5.2 Design Methodology

1. Disk Loading

Disk Loading (DL) is obtained by a curve fitting approach by collecting the data of similar category eVTOLs and helicopters. Although helicopters are mostly mono-rotor systems, the primary reason for using them for the estimate is the unavailability of the dimensions of large number of eVTOLS which also belong to a similar weight class as required in the RFP. From [1] we observed that the Disc loading of an eVTOL is approximately 3.5 times that of a helicopter of similar weight class.

- (a) A scatter plot of the disk loading vs. weight of similar category helicopters is plotted (figure 15), as mentioned in [8], a polynomial curve fit is generated. The polynomial curve relates DL and $M^{0.4215}$, which is well in accordance with the theory given in [8].

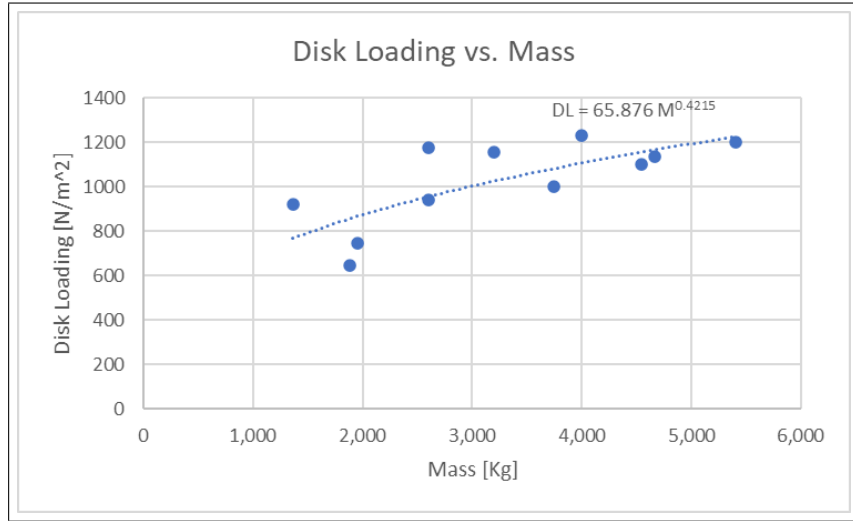


Figure 15: Disk Loading vs. Mass

2. Rotor Radius

From the disc loading the rotor radius is calculated using the formula to get a ball park value

$$R = \sqrt{\frac{W}{N\pi DL}} \quad (21)$$

From the weight distribution table [11], a simple equilibrium analysis about the CG shows that the rotors in the wings have to lift 30,000 N and that in the tails have to lift only 5,000 N. These values are then fed into the above equations to calculate a rough estimate for rotor radius. By imposing additional dimensional constraints from the wing, the radius of rotors in the wing is chosen to be 0.625 m. The radius of the rotors in the empennage is 1.25 m.

3. Tip speed

A higher tip speed can be achieved by only changing the angular speed of the rotor, as the radius dimension is frozen from the above calculation. A higher angular velocity can reduce the torque for a constant power $P = \Omega Q$, lower torque results in a lighter gear box and simpler design. But two major constraints are compressibility effects and noise. The maximum allowable value of tip speed is 0.72 Mach but a more conservative value of 0.652 is chosen for safety operations. Accordingly a maximum angular velocity of 310 rad/s and 170 rad/s is required by the rotors inside the wings and the empennage respectively. These values are more than sufficient for eVTOL to lift-off in 30 seconds.

- (a) Using the value of angular velocity the thrust coefficient C_T is calculated from

$$C_T = \frac{T}{\rho \times A \times V_{tip}^2} \quad (22)$$

4. Solidity (σ) and Chord length(c):

$$\sigma = \frac{bcR}{\pi R^2} \quad (23)$$

An important limitation on solidity is the limited value of blade loading (C_T/σ). From [10] the limit on the blade loading is chosen as 0.16 instead of 0.12 which was earlier used in MTR, the value of sigma is directly inversely proportional to the aspect ratio (defined as R/c). Higher AR implies a smaller chord, which requires lesser material and hence lower mass but a very high AR can also result in severe structural damage. Generally, AR lies in the range b/w 4 to 20. Solidity also affects the rotor performances significantly. The mean lift coefficient $\bar{C}_l = 6 \times C_T/\sigma$, is inversely proportional to solidity, so a low solidity gives a low stall margin which is undesirable. But a low sigma also decreases weight of the rotor system.

5. Number of blades (b): From the constraint on blade loading the minimum number of blades required to follow the constraint is 5. More than 5 would only increase the weight of the system unnecessarily, so b was chosen as 5 finally.

Parameter	Minimum		Maximum	
	Value	Limit	Value	Limit
empennage Rotor Radius	1 m	Hovering Power	1.32 m	empennage Sizing
Wing Rotor Radius	0.5 m	Hovering Power	0.75 m	Wing Sizing
empennage Rotors (Ω)	120 rad/s	Blade Loading	200 rad/s	Noise and Compressibility Effects
Wing Rotors (Ω)	275 rad/s	Blade Loading	330 rad/s	Noise and Compressibility Effects
Blade aspect Ratio	6	Low efficiency	20	Structural Limit
Number of Blades	5	Blade Loading	8	Weight

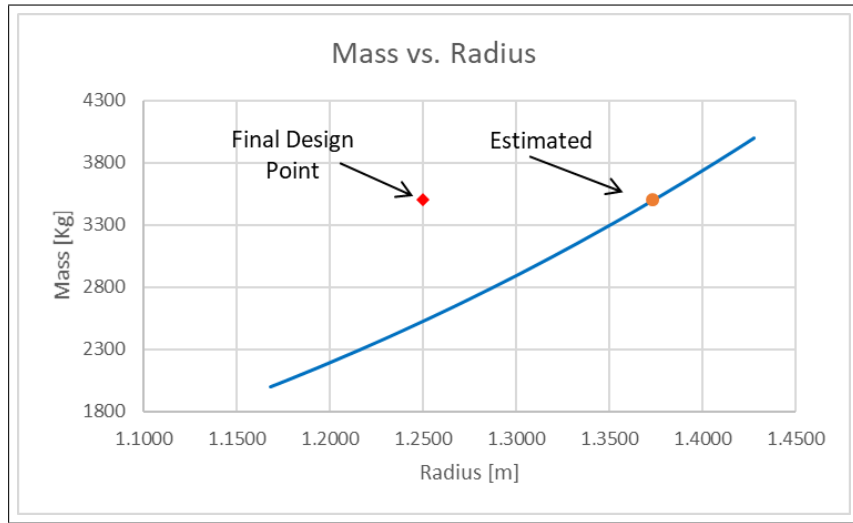


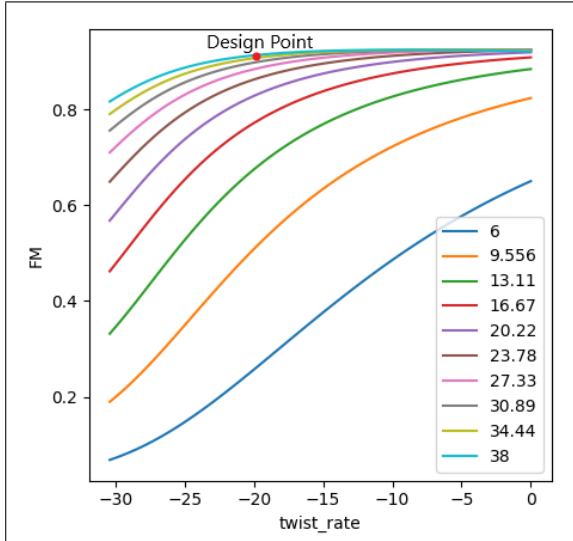
Figure 16: Mass vs. Radius

Each rotor in the wing requires to generate about similar magnitude of thrust as the rotors in the tail, this decreased the blade planform choices considerably for the wing rotors. Hence simple rectangular planform with minimum twist rate is proposed for wing rotors.

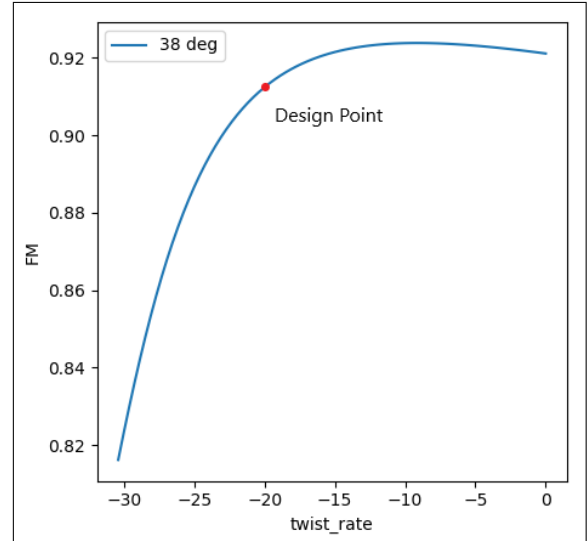
Blade Parameters	σ	0.1592
	R_{tail}	1.25 m
	R_{wing}	0.625 m
	C_T (empennage rotors)	0.0212
	C_T (Wing rotors)	0.0668
	V_{tip}	195 m/s

Table 4: Blade parameters

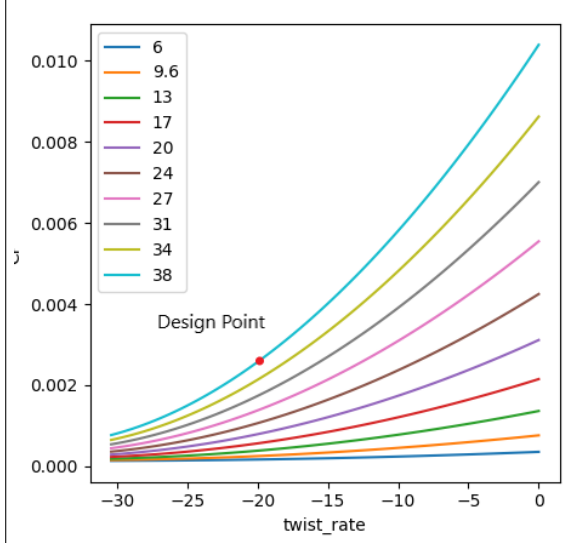
5.3 Blade Planform for Rotors in tail



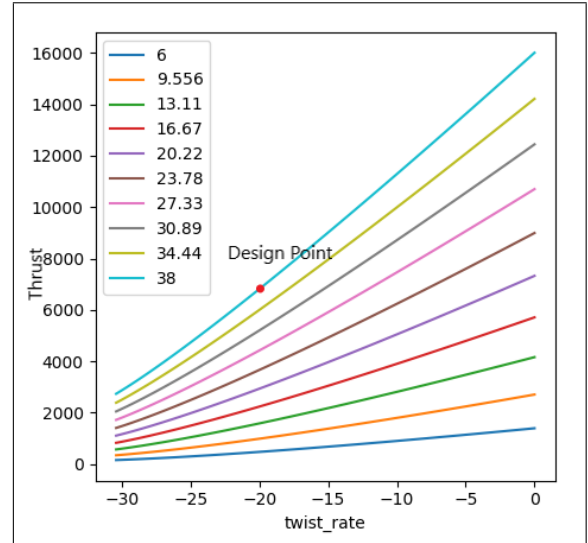
(a) FM vs. θ_{tw} with varying θ_{root}



(b) FM vs. θ_{tw} for the design point



(c) CP vs. θ_{tw} for the design point



(d) Thrust vs. θ_{tw} with varying θ_{root}

$$FM = \frac{C_{P,induced}}{C_{P,induced} + C_{P,profile}} \quad (24)$$

$$C_P = k_{int}C_{P,induced} + C_{P,profile} \quad (25)$$

$$P_{total} = 2 \times (C_P \rho A V_{tipspeed}^3)_{tail} + 8 \times (C_P \rho A V_{tipspeed}^3)_{wing} \quad (26)$$

k_{int} accounts for the interference factor in coaxial rotors. A is the area of the actuator disk, a pair of coaxial rotors in the empennage and 4 pairs inside wings. The effective angle of attack $\alpha_{effective}$ is well below the stall angle at all the radial locations, in addition the $\alpha_{effective}$ is around $\alpha_{(L/D)max}$ at $\frac{r}{R} = 0.8$ at which there is maximum downwash along the blade, this ensures lesser profile loss close to the tips and also higher lift.

$\theta_{tw,tail}$	-20^0
$\theta_{root,tail}$	-38^0
Taper ratio($r_{root,tail}/R$)	0.7152
$\theta_{tw,wing}$	-8.73^0
$\theta_{root,wing}$	-50^0
Taper ratio($r_{root,wing}/R$)	1.00

Table 5: Geometric Parameters

FM_{tail}	0.912
$C_{Ptail,hover}$	0.001
FM_{wing}	0.92
$C_{Pwing,hover}$	0.0159
$P_{total,hover}$	1290 kW

Table 6: Performance Parameters

The C_T required to hover for rotors in empennage is 0.0134 and for that in wing it is 0.0597, but the above calculation has been performed by keeping in mind that the eVTOL needs to accelerate upwards prior to hover phase.

5.4 Blade Structural Design

A basic structural analysis is done taking the surface of the blade as the shell elements and the contribution of one blade for total lift as a uniformly distributed load, the effect of centrifugal force due to the revolution of the blades and the rotor to be fixed at the hub(i.e.; a cantilever beam problem) and an analysis is performed to get the deformations and the stress distributions. The material used for blades is Woven Carbon Epoxy with stainless steel erosion strip at the leading edge of the blade. The results are as shown in figure 17 to 21.

This simulation shows that thickened blade surface alone isn't strong enough to resist the bending loads and hence there is the necessity of using some reinforcement to the blades by adding a spar. A better simulation can be performed

when we have the exact pressure distribution over the blade which would be more concentrated at around the center than the tip.

We can say that the deformation we obtained here are kind of an over estimation of what we would actually be seeing in a more accurate analysis as the lift force is more around the center than the tip which decreases the deflection. Also the consideration of the lift to be acting upward is not precise, because in reality it is produced by the difference in pressure on the upper and lower surface which would them to deform differently and the net deformation would be a bit less than what we are seeing here.

In the case of the stresses what we see here are an underestimation, as there would be stress developed because the load is due to the pressure difference and the stresses would increase due to this.

This analysis can be taken as the starting point, a slight increase in stresses would still be in the limit of factor of safety 2, moving on we will try to modify the structural support accordingly to maintain the stresses around the limit and decrease the deformation so that high deformation will not bring effects on aeroelastic instabilities into the structure.

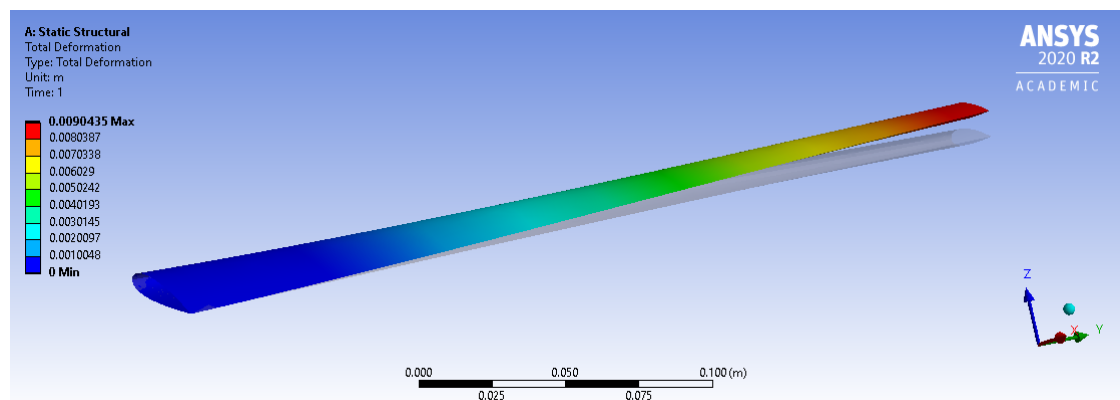


Figure 17: Total Deformation of the Blades

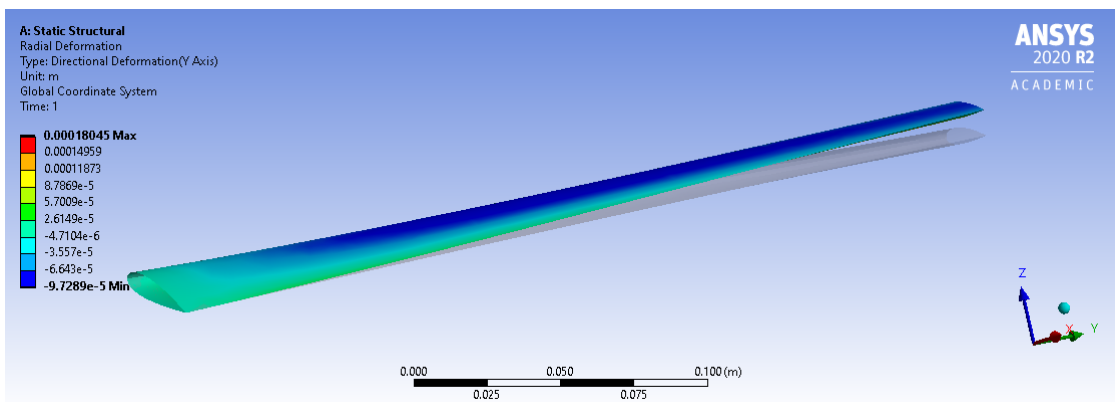


Figure 18: Radial Deformation of the Blades

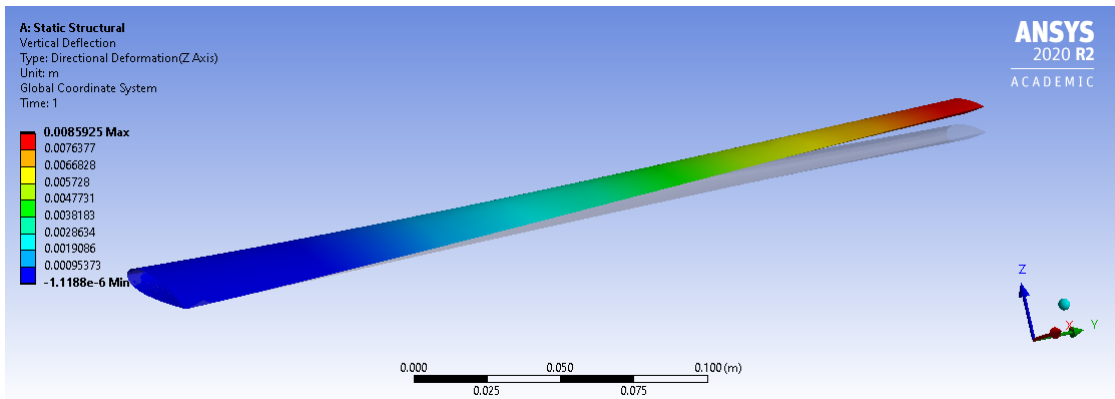


Figure 19: Vertical Deflection of the Blades

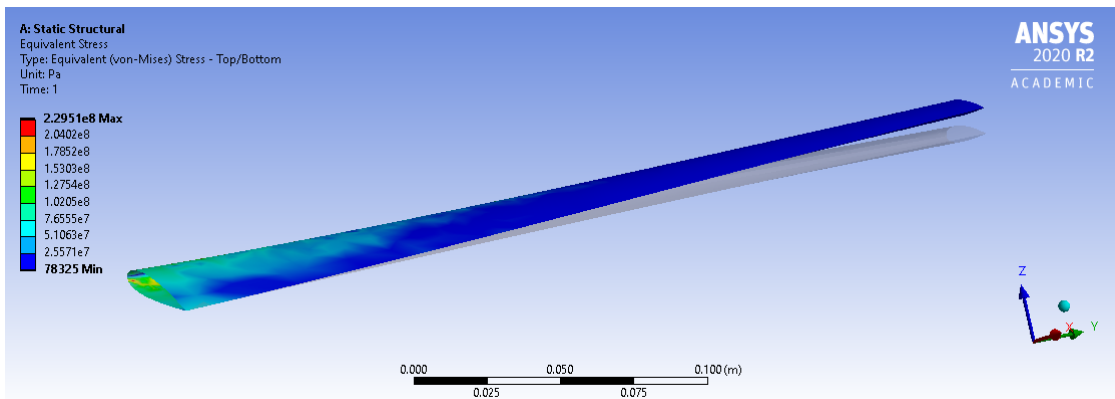


Figure 20: Equivalent Stresses in the Blades

6 Wing Design

The class of eVTOL for intercity commute at low mach number regime requires a high-lift configuration. The wing design was primarily driven by

- Long range requirement
- Enclosing the Rotors
- Efficient cruise

This chapter details the engineering analysis used to determine the aerodynamic and structural parameters of the wing. The following approach was chosen for wing selection.

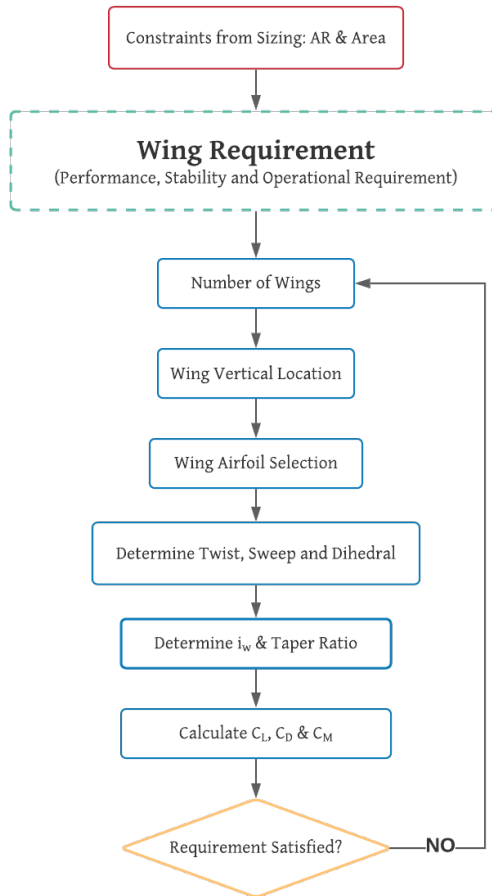


Figure 21: Wing Design Procedure

6.1 Airfoil Selection

The first criteria to short list airfoils is $C_{L,cruise}$. Cruising at an altitude of 1 Km from MSL, with a wing loading of **139** Kg/m^2 requires $C_{L,cruise}$ around **1.15** which is fairly high compared to other class of aircraft. Since the Aspect Ratio (**AR**) is **8**, the airfoil characteristics more or less resembles the wing characteristics. Eppler 423, S1223, NACA 9412 and the laminar airfoil NACA 67₁ – 1012 were considered for satisfying the $C_{L,cruise}$ criteria. Eppler 423 and S1223 have higher lift at a given AOA compared to all other airfoils. A rectangular wing comprising Eppler 423 at the tip and S1223 at the root was tested in xflr5 at 5.75 million Reynolds number. The highest $(\frac{C_L}{C_D})_{max}$ ratio of the wing is at negative AOA making it undesirable for cruise performance. The other airfoils considered were NACA 9412 and NACA 67₁ – 1012. The $(\frac{C_L}{C_D})_{max}$ of the rectangular wing, with NACA 9412 at the root and NACA 67₁ – 1012 at the tip, is at almost 0 degree angle of attack, making it attractive for cruise conditions. Additionally, this wing had higher lift to drag ratio than the previously selected E423 and S1223 airfoils at all AOA. The analysis was performed in **xflr5** with a **Lifting Line** solver. NACA 9412 was used at the root chord and NACA 67₁ – 1012 series airfoil was used at the tip chord, as the former has higher C_L than the latter at all AOA.

6.1.1 Laminar Airfoils

Laminar airfoils delay turbulent flow over the wing and maintain laminar flow to a specific chord length. Since the eVTOL is flying at about 5.75 million Reynolds number the flow is susceptible to turbulence over the wings which increases skin friction drag. Nomenclature of NACA 67₁ – 1012: The first digit 6 indicates the series. 7 indicates that at 70% of the chord the location of minimum pressure exists. Subscript 1 indicates that the airfoils maintains low drag 0.1 above and below design lift coefficient. 10 indicates $C_{l,design} = 1.0$ and 12 stands for thickness to chord ratio in percentage. An additional parameter a is also associated with the airfoil. $a = 1.0$ indicates that the flow over the airfoil is fairly laminar throughout the chord length.

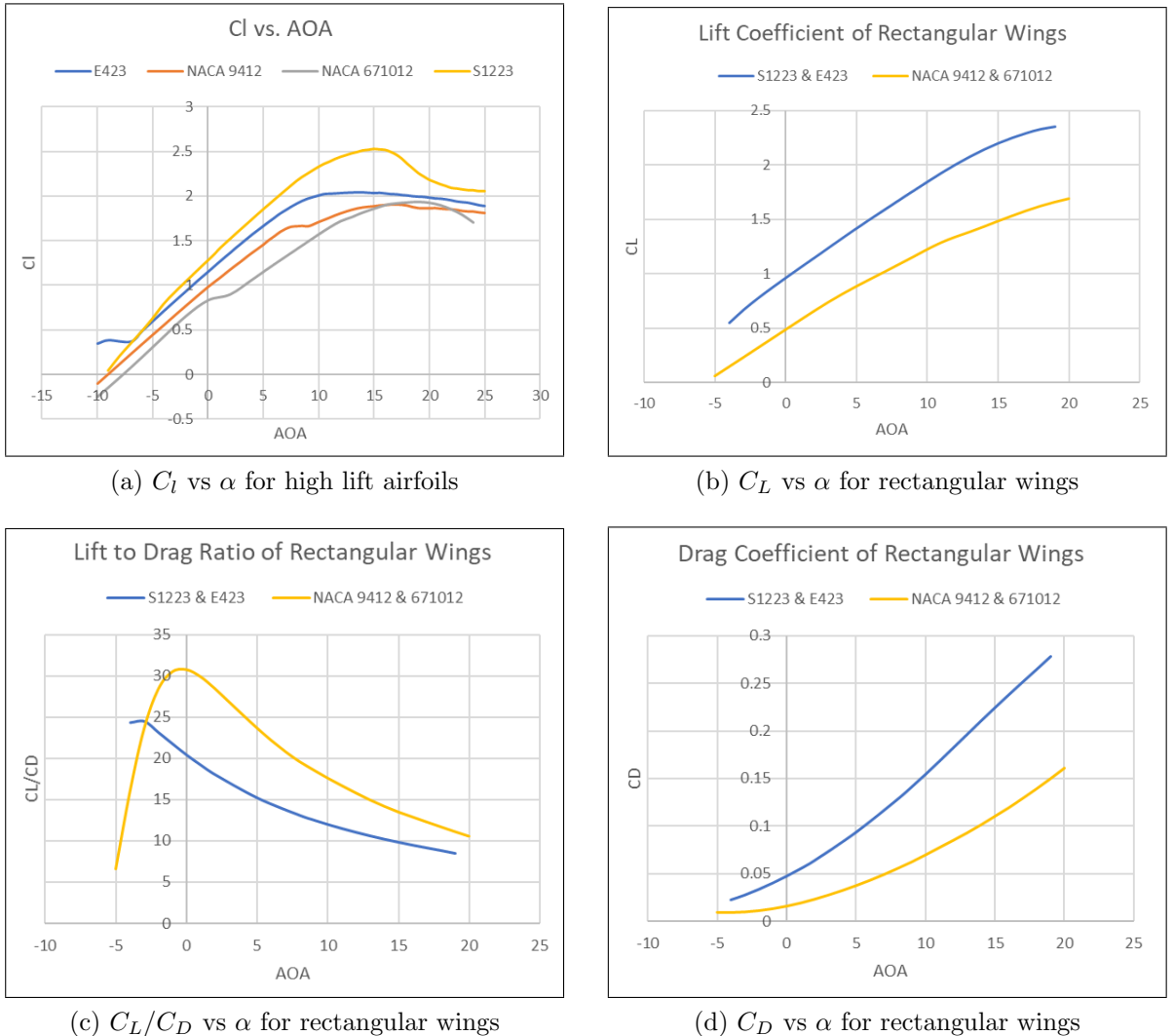


Figure 22

6.2 Wing parameters

A sweep of about 10° was introduced for aesthetic purpose. After a rigorous flow simulation in ANSYS Fluent (detailed in section 10), 0° twist and a wing incidence angle 5° with respect to the fuselage was the only configuration to satisfy the $C_{L,cruise}$ criteria at 0° . The $(\frac{C_L}{C_D})_{max}$ of the total aircraft is **15** which is also at 0° . The placement of the rotors inside the wing was an additional constraint due to which taper ratio of 1 was finally chosen. To quote the exact words of *Coleman* [2], who did a survey, “*the greatest gains were made up to $H/D = 0.05$; thereafter, no*

practical gains resulted with increasing separation distance". Hence a rotor spacing of $\mathbf{H/D = 0.05}$ was finalized. The spacing between the rotors is $\mathbf{H = 6.25 \text{ cm}}$. The wing has a $t/c = 12.09\%$ at the root with root chord being 1.5 m . This gives $t = 18 \text{ cm}$ which is sufficient for enclosing the rotors along with the hub and the motors. The wing is blended with the fuselage to reduce the interference drag and winglets were installed to reduce the induced drag. The middle section of the wing shown is enclosed inside the fuselage and the area mentioned in the table below is the projected area of the exposed wing.

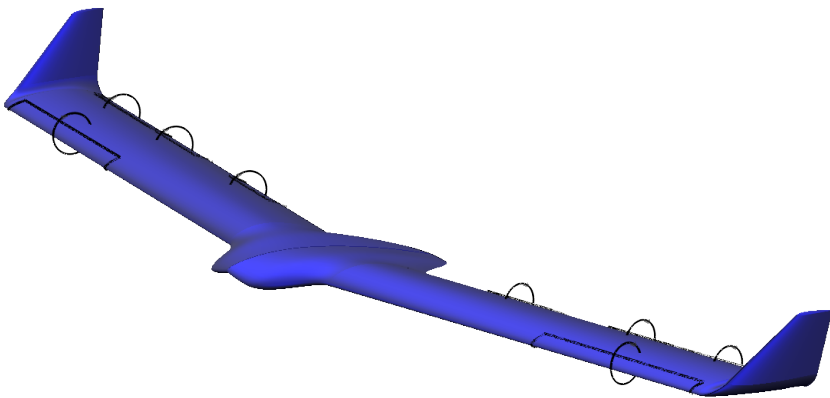


Figure 23: Aerodynamic Design of Wing

Wing Parameters	
Span	12 [m]
Mean Chord	1.5 [m]
Aspect Ratio AR	8
Wing Projected Area	18 [m^2]
Airfoil at Root Chord	NACA 9412
Airfoil at Tip Chord	NACA 67 ₁ – 1012
Twist	0 ⁰
Taper Ratio λ	1
Sweep Λ	10 ⁰
Oswald factor e	0.9

6.3 Wing Structure

Wing being the major component of aerodynamic lift and also the placement of the take-off rotors, its structure needs to be light weight and strong enough to sustain the appearing loads. The major components of the wing structure are the Spar, Ribs, Stringers and the Outer skin. This section deals with all the structural analysis of the entire wing.

6.3.1 Wing Structural Design

We start our structural design of the wing with the spar which is the main bending load carrying member. From Beam theory we have,

$$\sigma = \frac{M}{I} z_{max} \quad (27)$$

Where, σ is the maximum stress in the spar, M is the maximum bending moment, I about the neutral axis and z_{max} is the maximum distance of the cross-section from neutral axis.

One of important criterion is to avoid entering the plastic regime so that there is no permanent deformation of the structure during flight. So, considering the maximum stress attained is the Yield Stress(σ_y) and the cross-section of the spar is a rectangle of length(h), we get the minimum thickness(b) to avoid plastic deformation as,

$$b = \frac{12}{h^3} \frac{M}{\sigma_y} z_{max} \quad (28)$$

From the above estimated minimum thickness(b) the tip deflection considering a uniform load(P) is obtained as,

$$\delta_{max} = \frac{PL^3}{EI} \quad (29)$$

Where, E is the Young's Modulus of the material used for spar and L is the length of the wing from midplane. From the airfoil selection we have the maximum thickness as $18cm$, we will have an effective height of the cross-section after considering the thickness of the wing skin as $\approx 16cm$. We have the wing span from the mid plane of the fuselage as $7m$. Using the above equations the behavior shown by different materials is as shown in Table 7

Material	σ_y [MPa]	Density [kg/m ³]	E [GPa]	b [m]	d [m]	Mass [kg]
Structural Steel	250	7850	200	0.073	0.223	642.82
Stainless Steel	207	7750	193	0.088	0.192	766.47
Aluminium Alloy	280	2770	71	0.065	0.705	202.53
Magnesium Alloy	193	1800	45	0.095	0.766	190.93
Titanium Alloy	930	4620	96	0.020	1.731	101.70
Carbon epoxy woven(0/90) (230GPa) prepreg	55	1420	61	0.335	0.159	532.42
Carbon epoxy woven (0/90)(395GPa) prepreg	83	1480	93	0.220	0.162	365.04

Table 7: Spar Details for Different Materials

This table is obtained for a P of $26,000N$ corresponding to a Lift force of $52,000N$ and a Bending Moment M of $77989N\cdot m$. We can see that Titanium alloy weight very less compared to other materials and the elastic deformation is pretty high. Taking a Factor of Safety of 1.75 for the yield stress we will take Titanium alloy of width $36mm$ for the wing spar.

For the stringers going throughout the span connecting the ribs Carbon fiber UD (395 GPa) pre-preg is chosen as it is light weight and the primary loads are axial loads. The wing skin is a case of plane stress so the best suitable material is something which is strong for the 2D stresses. Hence, Carbon Fiber woven(0/90) (395 GPa) pre-preg is selected for the wing skin which is $4.5mm$ thick. Finally for the ribs($5cm$ thick) whose primary objective to maintain the airfoil cross-section through out the wing and also are placed such that the column length of stringers decrease in turn avoid buckling of stringers and upper skin due to the compressive stresses caused when the wing is deflected. So a simple low density polymer like polyethylene was taken for starting analysis and it works without any high stress concentration and any plastic deformation. With this we have sufficient data to do the structural analysis for take-off and cruise.

Component	Material Used	Young's Modulus [GPa]	Density [kg/m ³]	Yield Strength [MPa]	Ultimate Strength [MPa]
Spar	Titanium Alloy (Isotropic)	96	4620	930	1070
Ribs	Polyethylene (Isotropic)	1.1	950	25	33
Stringers	Epoxy Carbon UD (395 GPa) Prepreg	209	1540	188	1979
Skin	Epoxy Carbon Woven (0/90) (395 GPa) Prepreg	92	1480	83	829

Table 8: Material Assignment for Wing Structure

6.3.2 Structural Analysis of the Wing

For the structural analysis we made a CAD model on SpaceClaim based of the discussed design criteria and the analysis is performed using ANSYS.

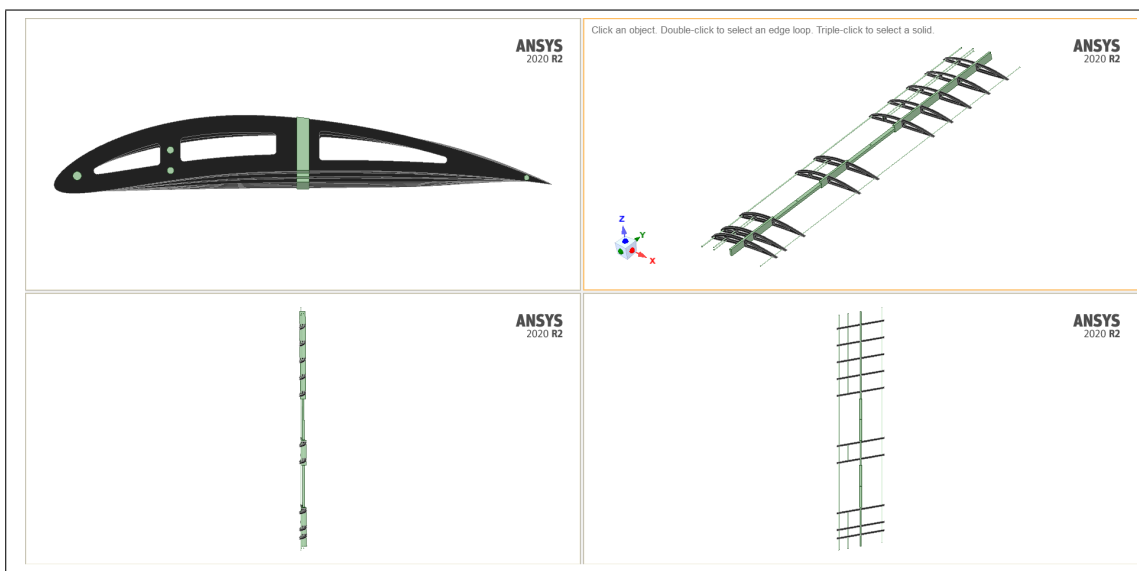


Figure 24: Wing Structure

First a static structural analysis is performed for Take-Off case when each of the coaxial rotors setup produce a lift of 7500N and the details of setup and analysis are shown in the following images

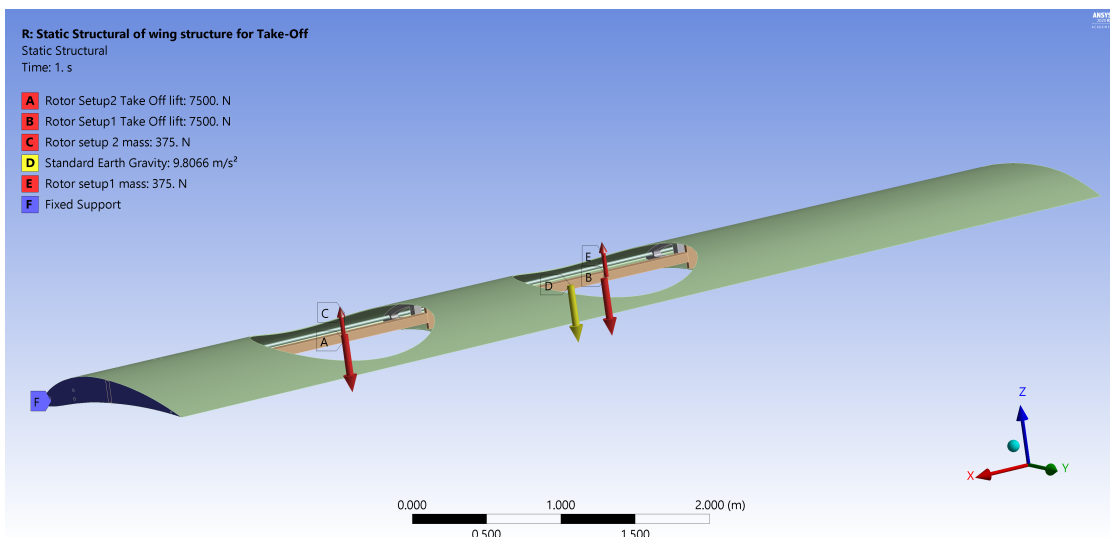


Figure 25: Analysis setup for Take-Off

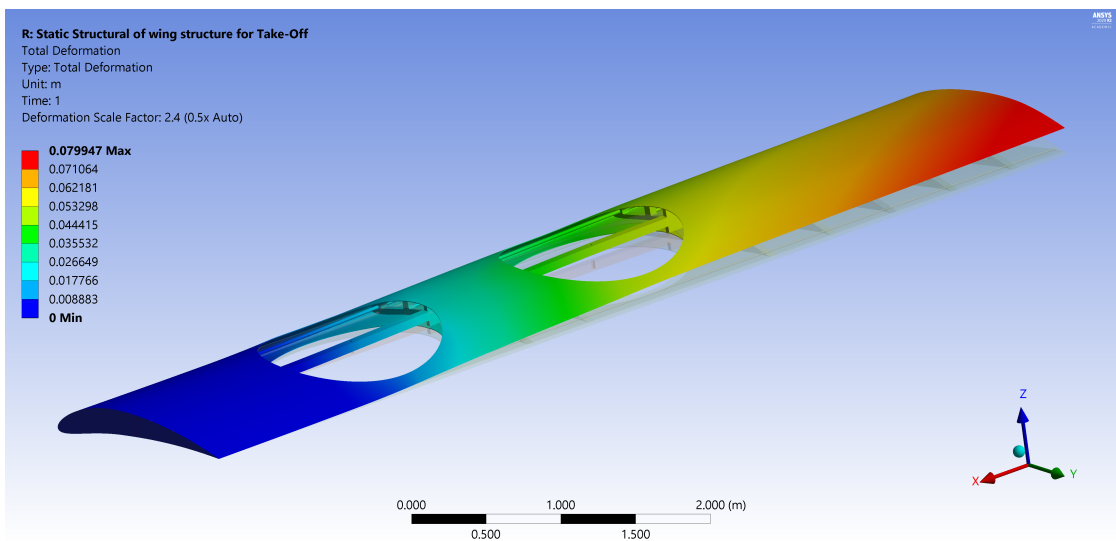


Figure 26: Total Deformation for Take-Off

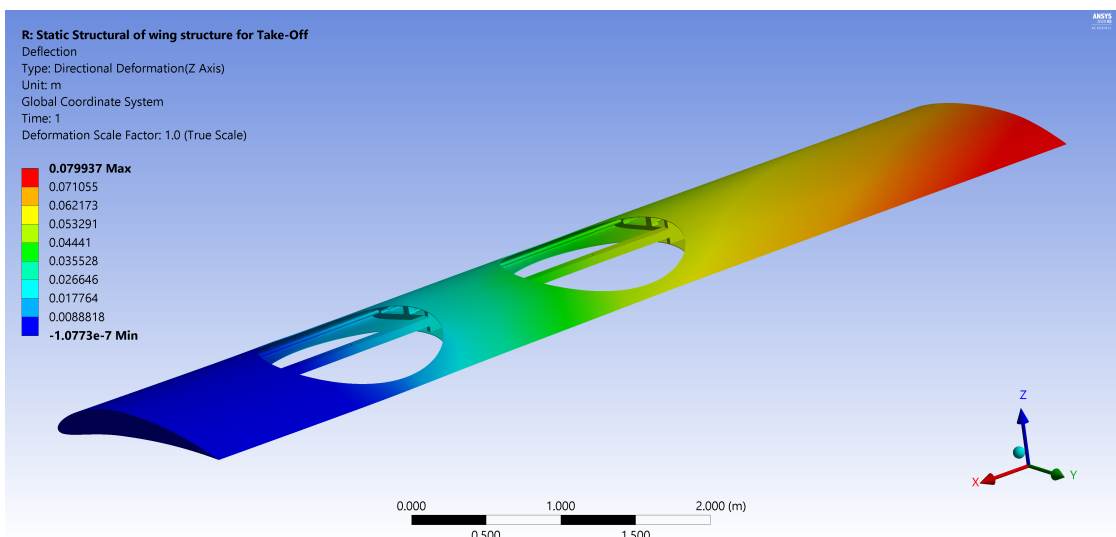


Figure 27: Deflection for Take-Off

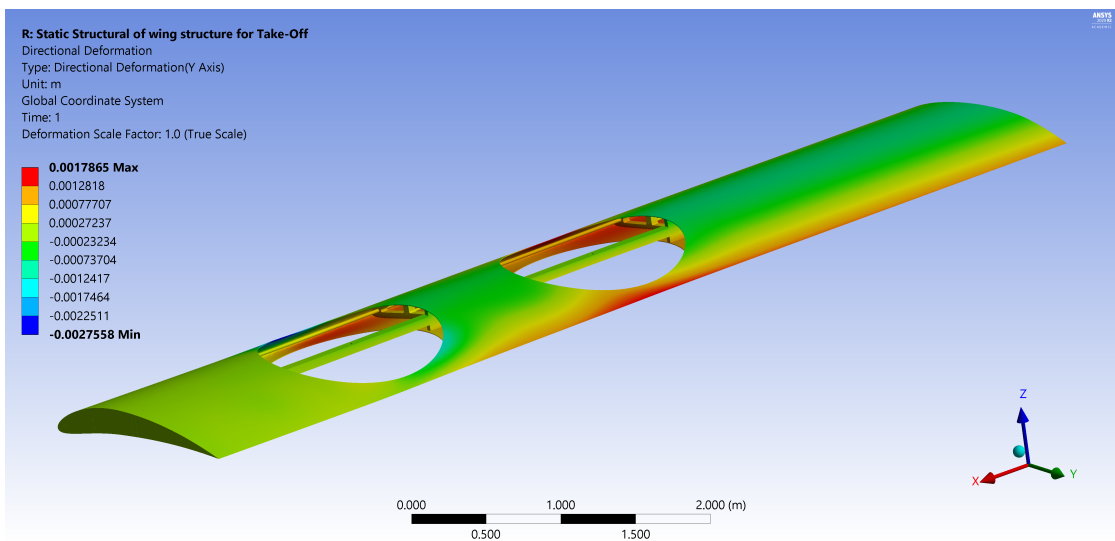


Figure 28: Directional Deformation(Y Axis) for Take-Off

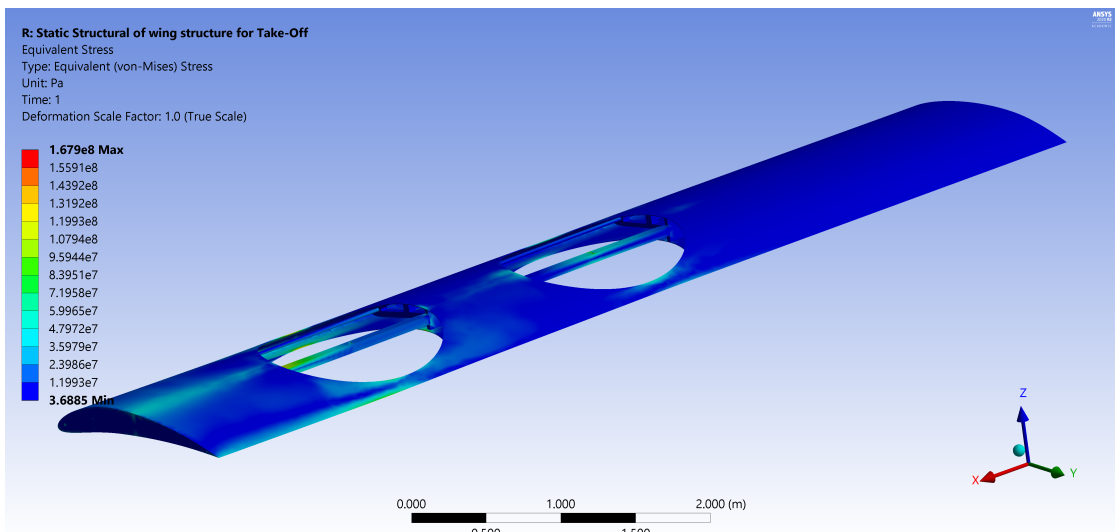


Figure 29: Von-Mises Effective Stress for Take-Off

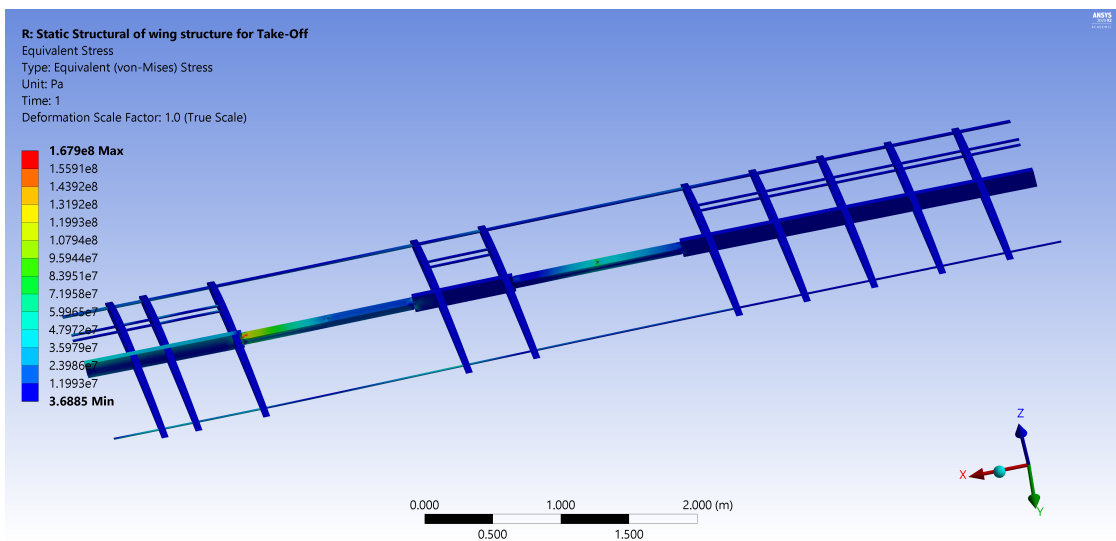


Figure 30: Von-Mises Effective Stress on the internal structure for Take-Off

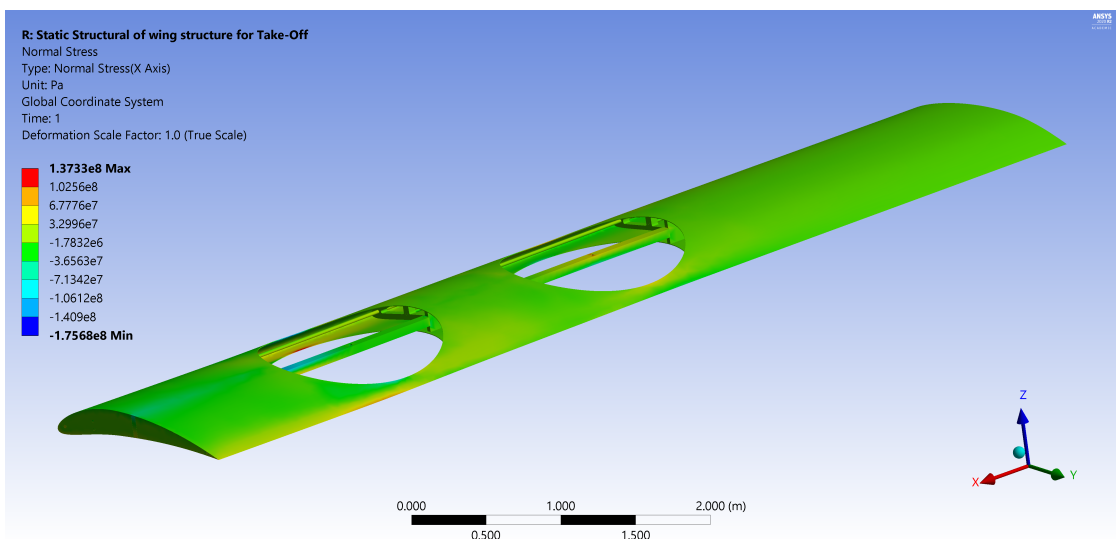


Figure 31: Normal Stress for Take-Off

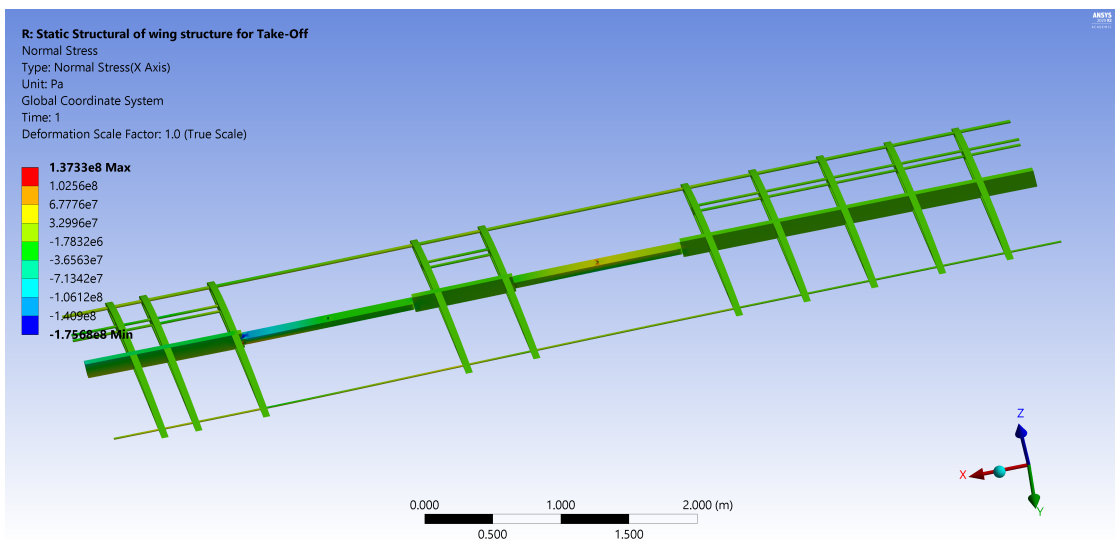


Figure 32: Normal Stress on the internal structure for Take-Off

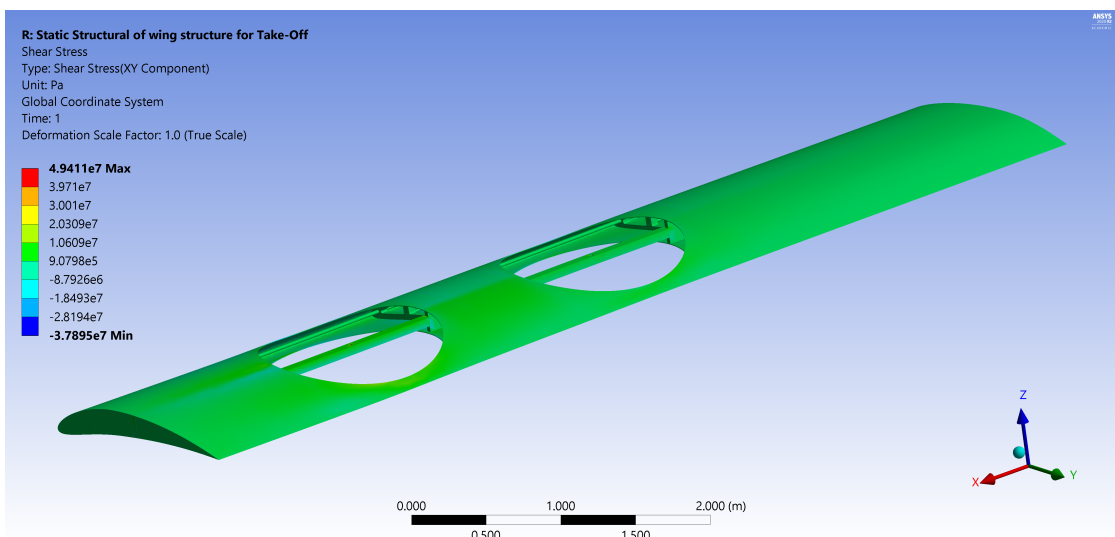


Figure 33: Shear Stress for Take-Off

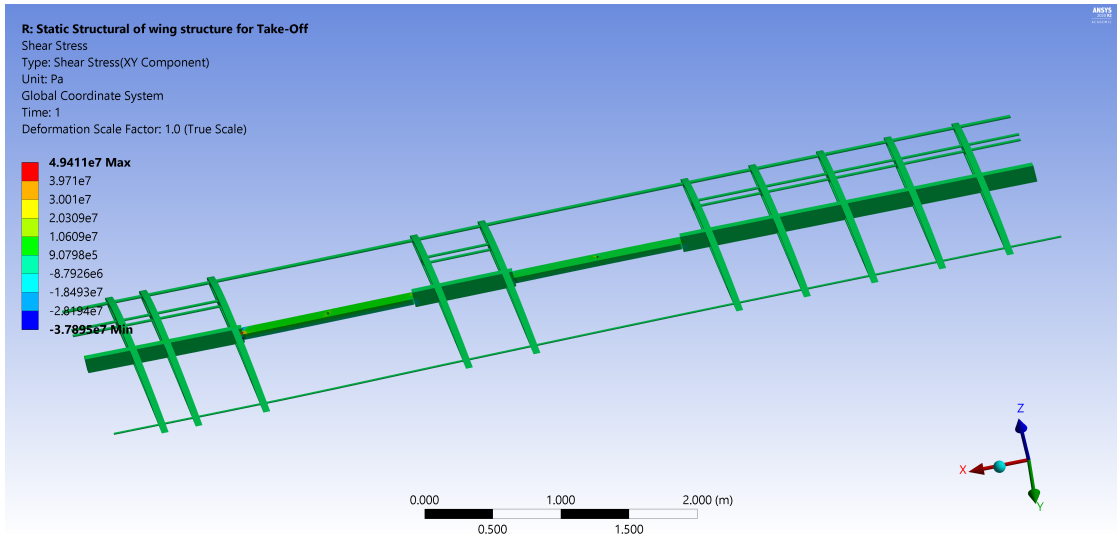


Figure 34: Shear Stress on the internal structure for Take-Off

From the analysis we can observe the maximum stress in in the spar and is well below the yield strength of Titanium alloy and deflection is around 8cm. Next analysis for cruise is done, the setup and analysis results are as follows,

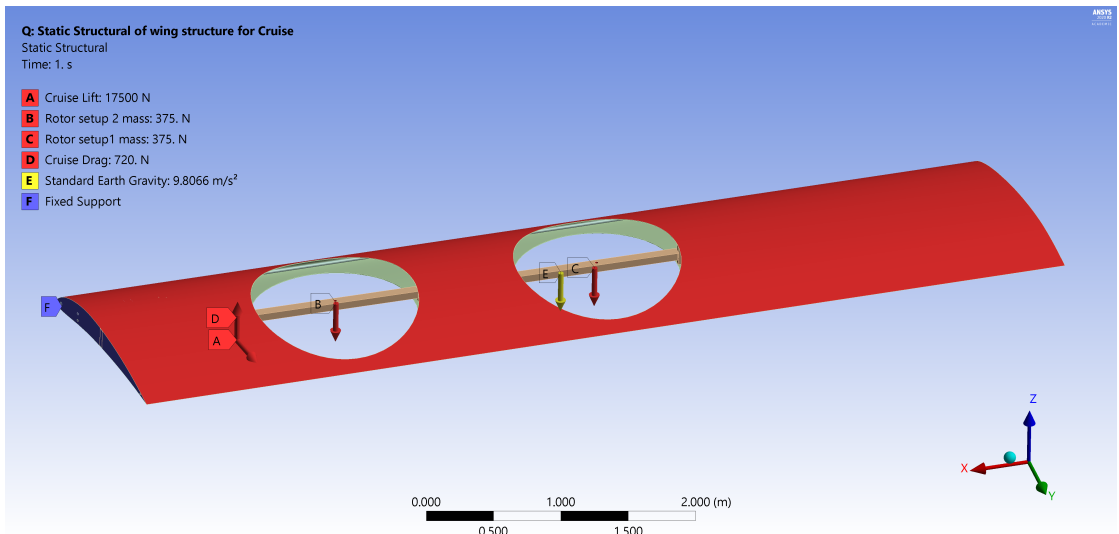


Figure 35: Analysis setup for Cruise

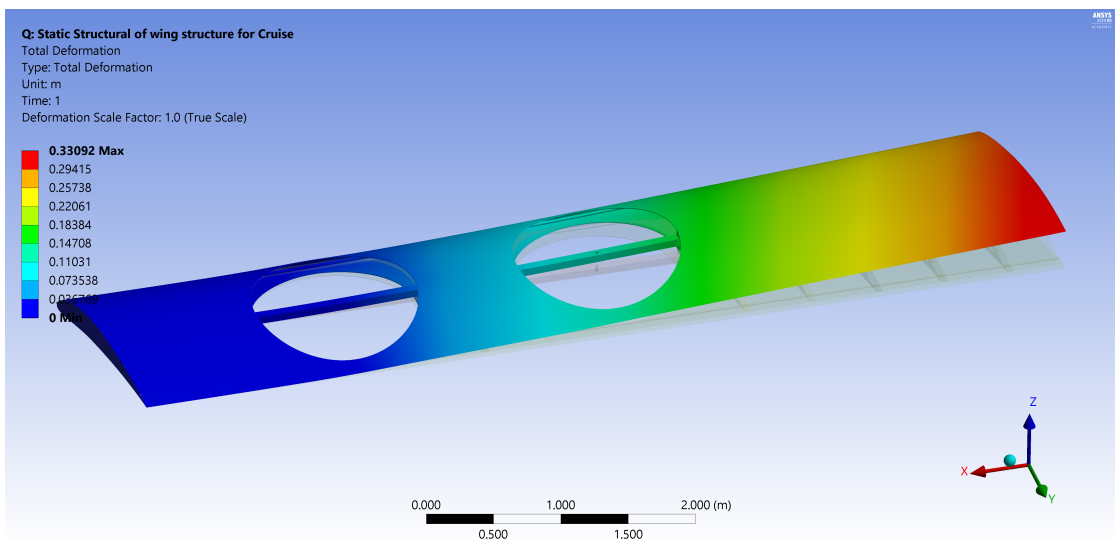


Figure 36: Total Deformation for Cruise

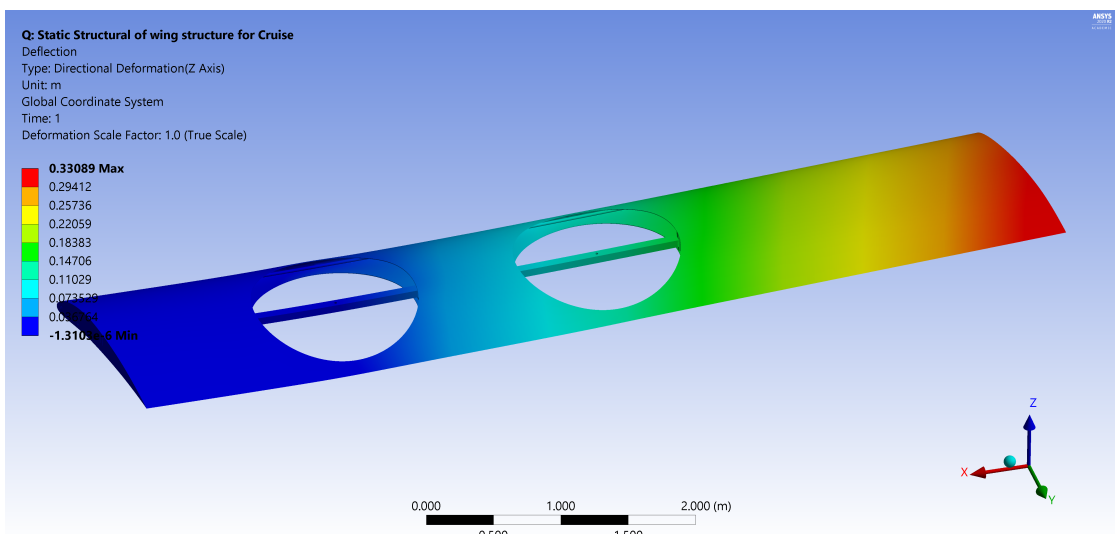


Figure 37: Deflection for Cruise

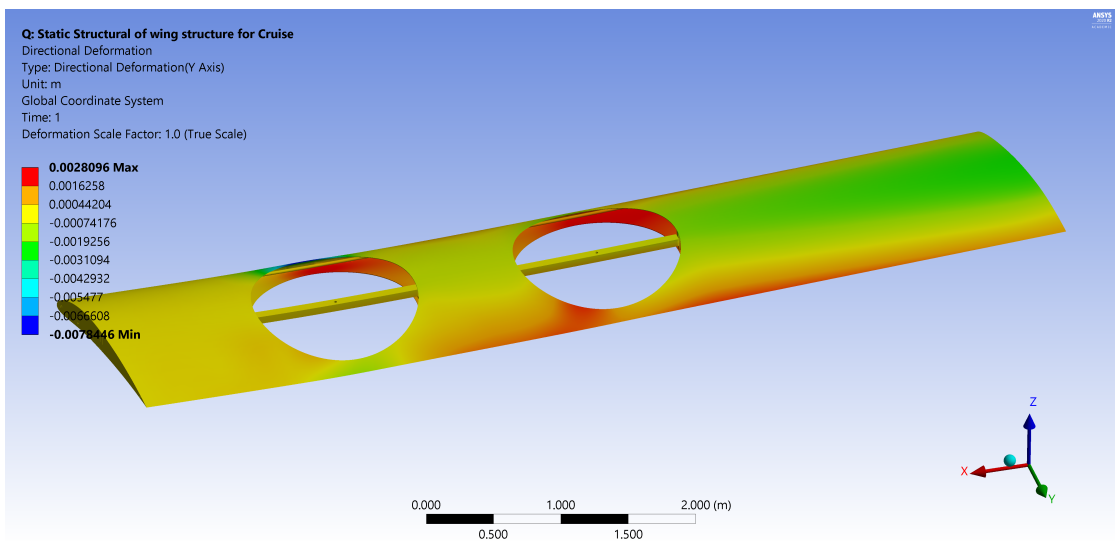


Figure 38: Directional Deformation(Y Axis) for Cruise

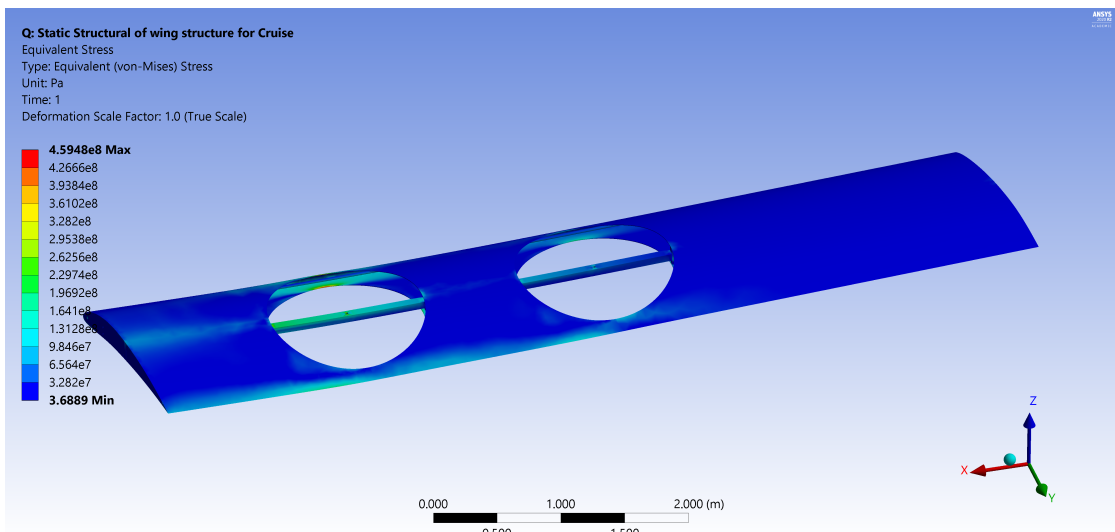


Figure 39: Von-Mises Effective Stress for Cruise

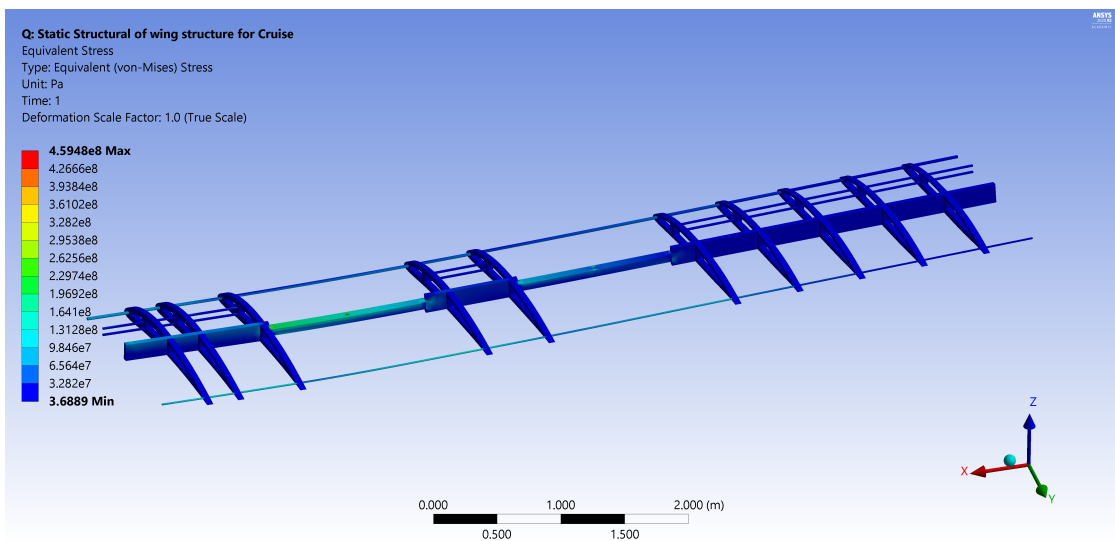


Figure 40: Von-Mises Effective Stress on the internal structure for Cruise

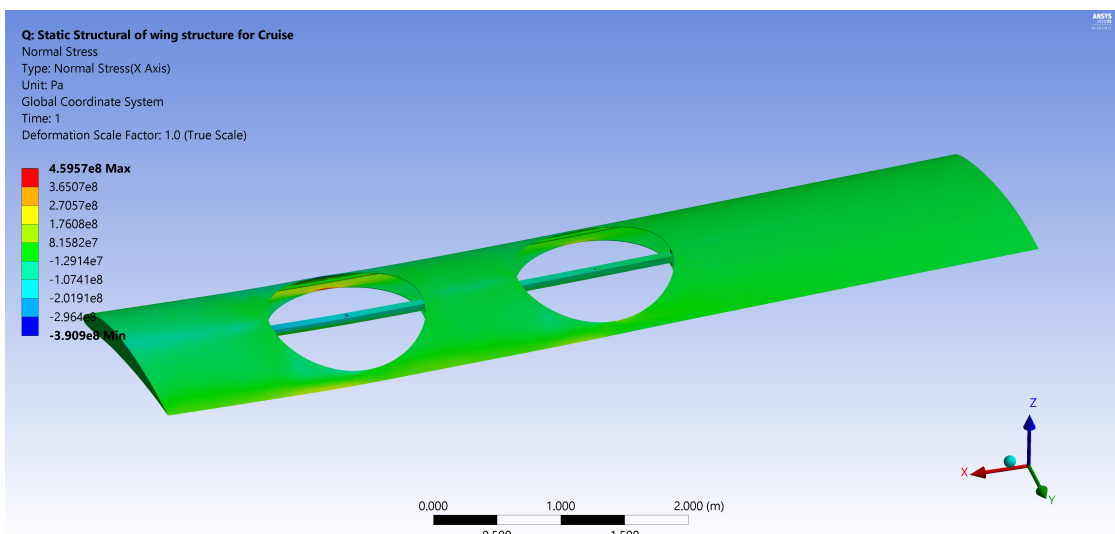


Figure 41: Normal Stress for Cruise

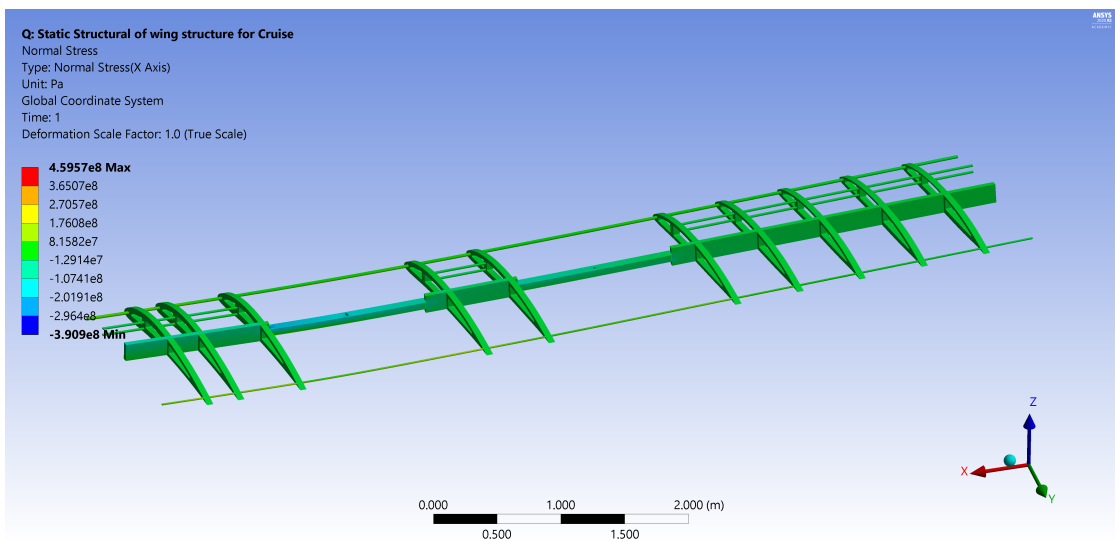


Figure 42: Normal Stress on the internal structure for Cruise

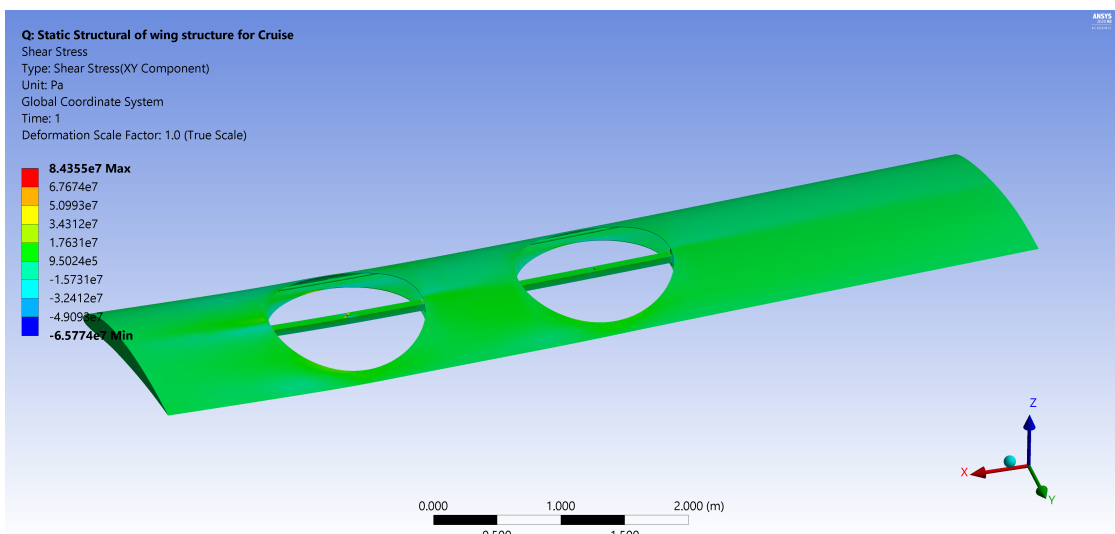


Figure 43: Shear Stress for Cruise

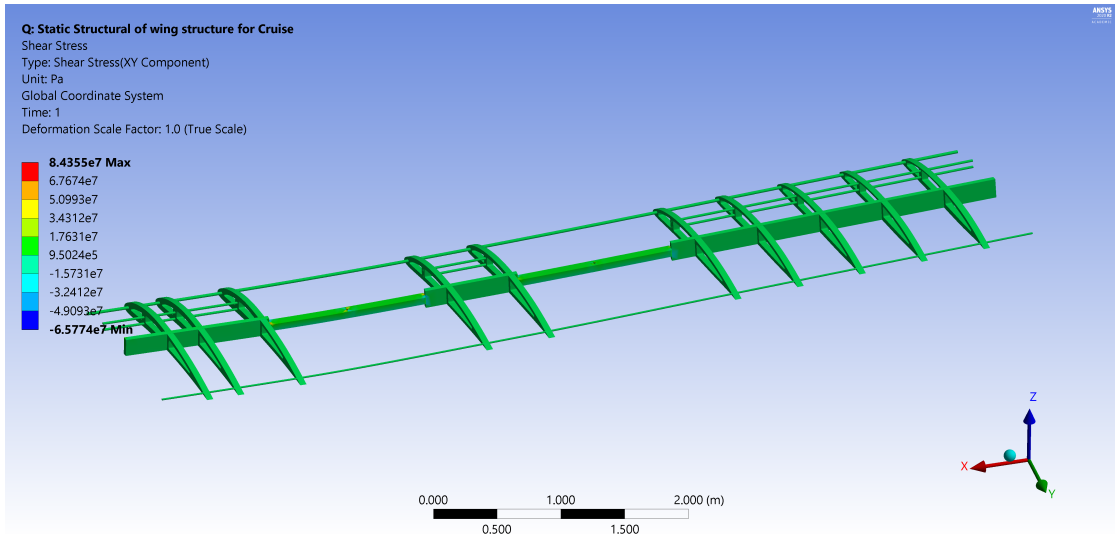


Figure 44: Shear Stress on the internal structure for Cruise

From the analysis of cruise we can conclude the spars, ribs are functioning as desired. In case of the outer skin in cruise analysis the cut-out done for rotor location shows more than desired stresses which might be problematic. This case is a direct analogy to the plate with the hole case, and one of features which will help us avoid any failure near the hole is the presence of the shutter mechanism. This mechanism will be deployed at cruise to cover the rotors and ensure that there is a complete airfoil at the rotor locations. The structural aspect of this mechanism is to have a closed structure which smoothens stress flow in the skin avoiding any stress concentrations, this will bring down the stresses below yield and the stress state would be similar to the skin on the rest of the wing. “Note: The structural analysis including the shutter mechanism was not performed at this stage because of its complexity ”

7 Fuselage design

The fuselage design is done using the constraints from the sizing which gives us the boundary box in which we should have our fuselage and we designed the the curvature to be such that we would get less drag as fuselage contribution to drag is of more priority than its contribution to lift.

The fuselage design is done by partitioning the total length of 8 meters it into 3 sections, one is the cockpit at the front occupying about 2.0 meters in length and then we have the cargo/passenger section with width of 1.9 meters, height of 2.1 meters and a length of 2.4 meters and the the third section is used for the storage of batteries and also as the moment arm for the pitch control by the tail.

The designed fuselage is as shown in the Figure 45 with an upward sweep of 20° and down sweep of 10° in the rear section(third section)

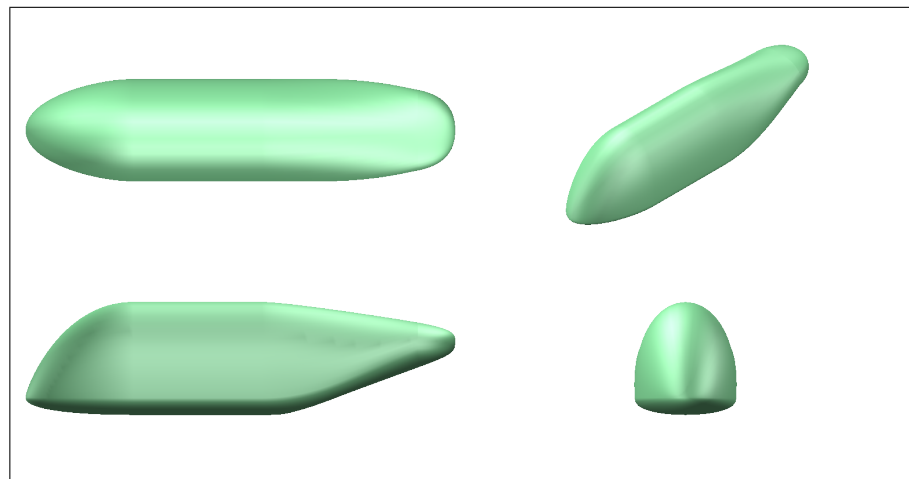


Figure 45: Fuselage Views

The fuselage presented here is modified from the one that was present in the MTR as the later suffered a lot of separation at the back. The modified fuselage has very low flow separation at its back and promotes lift even at higher angles of attack. The separation is predicted by the sudden change in the magnitude of wall shear stress over the surface of the fuselage, this is indicated by the contours as shown in the image below

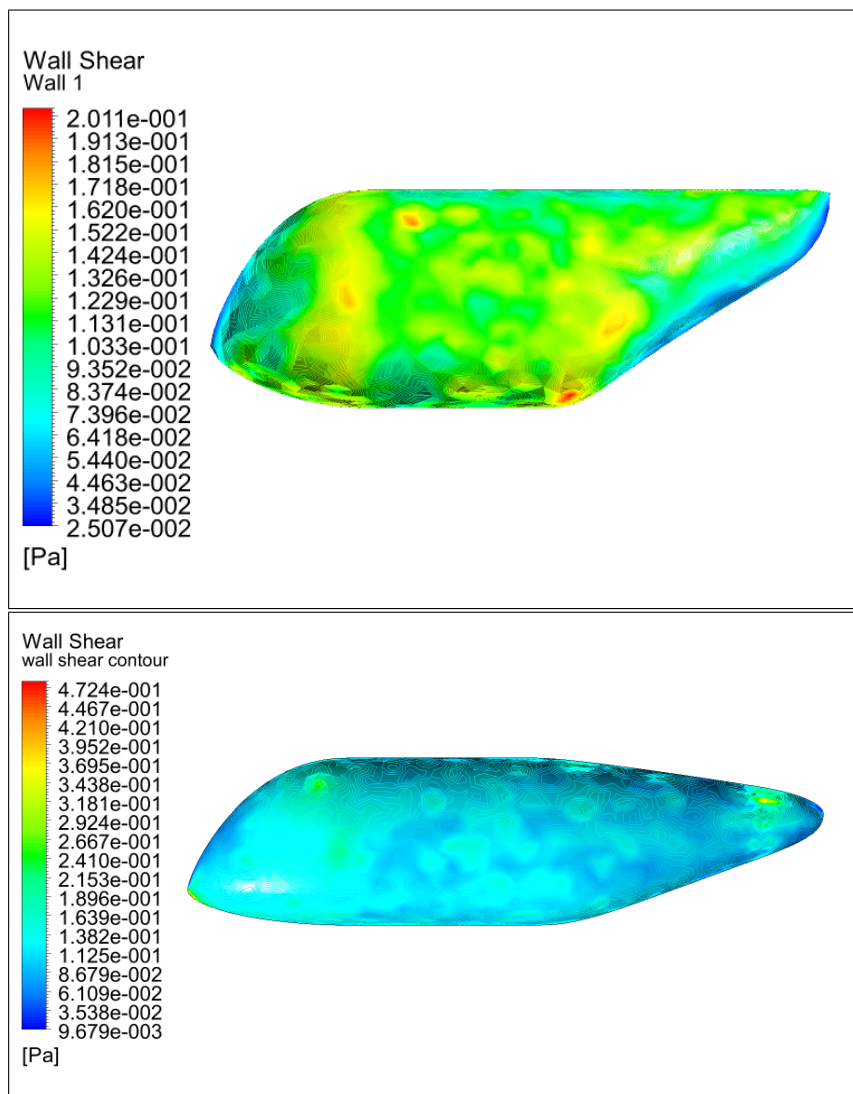


Figure 46: Fuselage Design Modification

7.1 Seating Arrangement and Layout

The seating arrangement in the fuselage is done to accommodate four passengers and one pilot and seating is as follows,

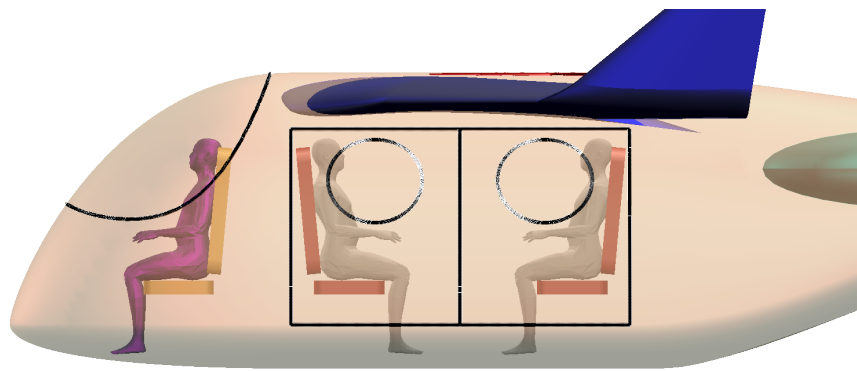


Figure 47: Seating Arrangement Side View

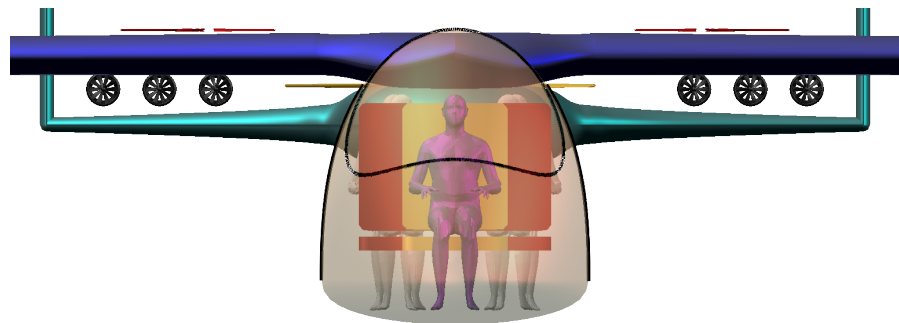


Figure 48: Seating Arrangement Front View

The doors to the passenger compartment are sliding doors with fibre glass windows which slide side-wards as seen in minibuses and vans, whereas the pilot compartment is isolated from the passenger compartment and the glass above him acts as an aircraft canopy seen in fighter jets and opens upward for the pilot to enter and exit.

Required $0.5m^3$ luggage space for passenger mode operations is allocated below the seats. Alternatively, we have $1.5m^3$ space between the seats for cargo mode operations. The seats can be reconfigured by folding them by 180° , giving additional free volume. It can be used for low-density payloads. Space is also allocated for the retractable landing gears which are deployed outwards by a motor connected to a rotating mechanism. See figure 49 for the details.

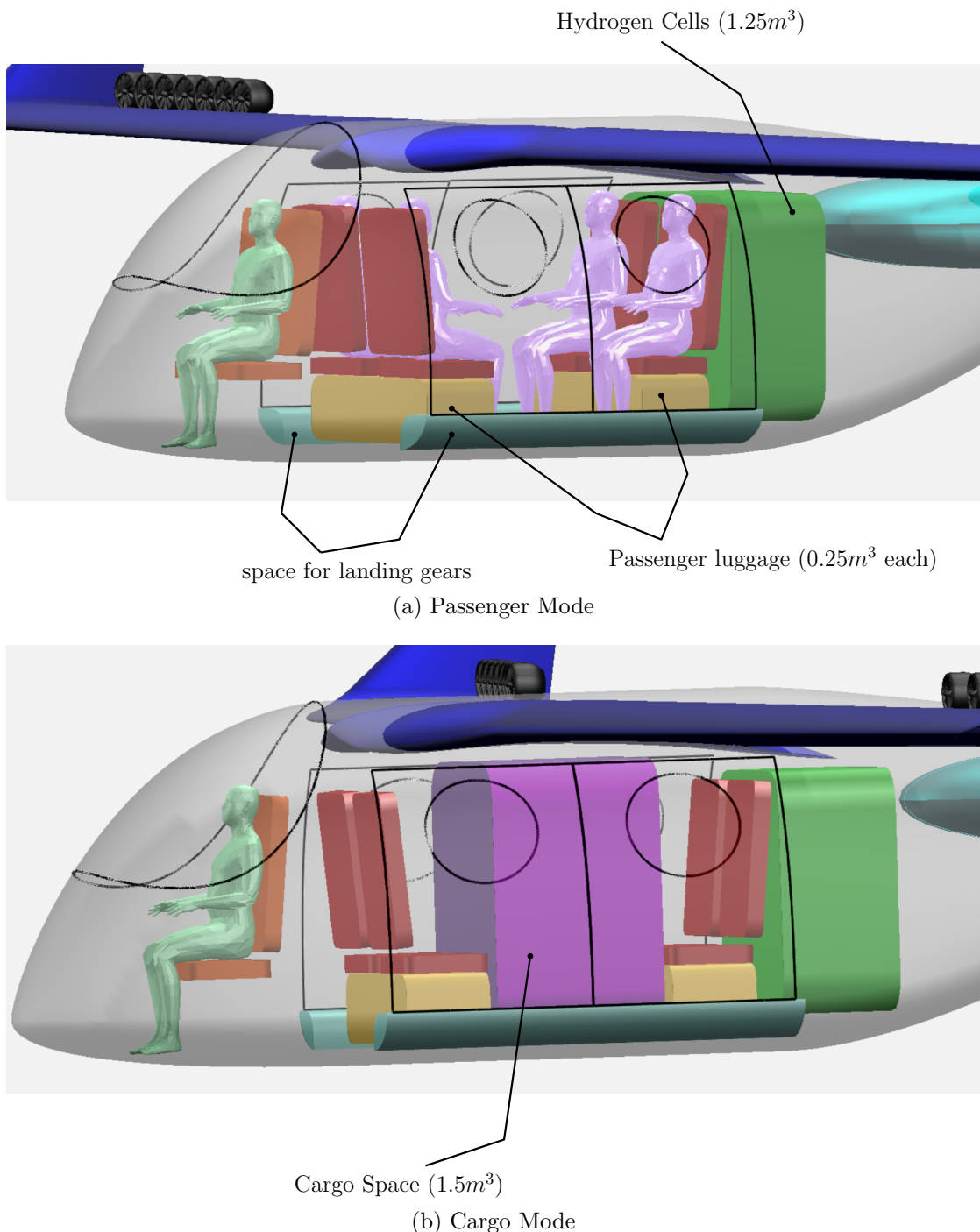


Figure 49: Space allocation inside the fuselage.

8 Tail Design

8.1 Design Considerations

To assist the vertical takeoff, it was decided to have a rotor in the horizontal stabilizer, as shown in figure 50. It rendered conventional tail design methodologies unusable. To circumvent this, we simplified the design process by calculating the horizontal stabilizers' design parameters using the traditional methods (discussed in the next sub-session). Then we modified the tail by adding the rotor at the center of the horizontal stabilizer while ensuring that area excluding the tail-rotor is equal to the value for conventional design.

8.2 Horizontal And Vertical Tail Volumes

The approach to design tail sections for this eVTOL was through using the concept of Horizontal and Vertical Tail Volume ratios. For a aircraft, they are defined in equation 30. Subscripts H, V, W refer to horizontal tail, vertical tail and the wing respectively.

$$V_H = \frac{S_H L_H}{S_W \text{MAC}}$$

$$V_V = \frac{S_V L_V}{S_{Wb}} \quad (30)$$

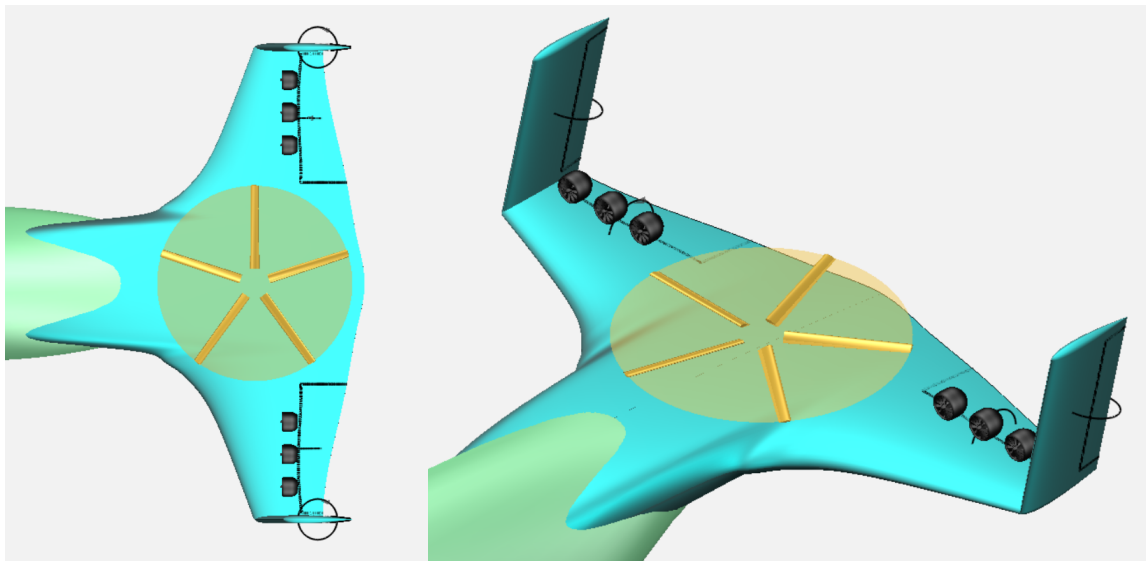
Reasonable values for V_V and V_H were chosen by multiple iterations until aerodynamic, stability and structural conditions gave decent results. The value of L_V and L_H were taken approximately the same and equal to 5.m . Table 9 gives us a brief overview of the horizontal and vertical tail dimensions.

Parameter	Value	Parameter	Value
Mean Chord length	140 cm	Mean Chord length	80 cm
Span	320 cm	Span	130 cm
Aspect Ratio	2	Aspect Ratio	3.25
Airfoil	NACA 0012	Airfoil	NACA 0012
V_H	1.37	V_V	0.63

(a) Horizontal tail

(b) Vertical tail

Table 9: Design parameters for the tail



(a) Top view

(b) Isometric view

Figure 50: Design of the tail with the rotor.

9 Final Design

As discussed in the earlier sessions we have come up with a final design. Figure 51 shows the OpenVSP model of the aircraft. Figure 52 shows different views for the aircraft. Rotors in the figure are for the representative purpose only, actual placement of the rotors (coaxial) is inside the wing with a cutout.

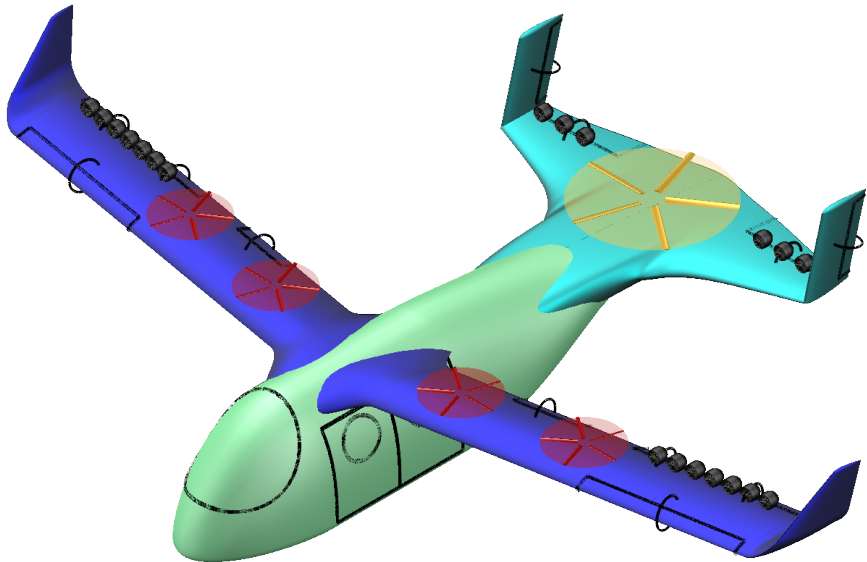


Figure 51: Final design of the aircraft

To talk about the design as a whole, it is a Lift + Cruise configuration eVTOL, which hovers using coaxial rotors and cruises using electric ducted fans with a large margin of safety. It uses HyPoint Turbo Air Cooled H₂ Fuel Cell technology as its power source. The passenger/cargo space is inter convertible. With 200km/hr cruise speed, this eVTOL can travel between cities upto 500-600 kms comfortably.

10 CFD Simulations for Aircraft

The flow simulation was performed in ANSYS Fluent Academic version whose license is provided by the Institute. The details about the complete simulation is detailed in this chapter which allowed us to calculate the lift, drag and moment coefficient of the entire aircraft accurately.

10.1 Grid and Mesh Quality

The grid size is an enclosure of $15 \times 15 \times 25$ meters. Since the aircraft is symmetrical about the longitudinal plane it was assumed that the flow would also be symmetrical. So only half the model was considered in order to decrease the computational time. The number of elements are about 3,72,000. A static mesh with an average element size of 5 cm was placed on the surface of the eVTOL. It should be noted that inflation layers could not be added to the surface, to accurately capture the boundary layer effects, due to limited computational resources.

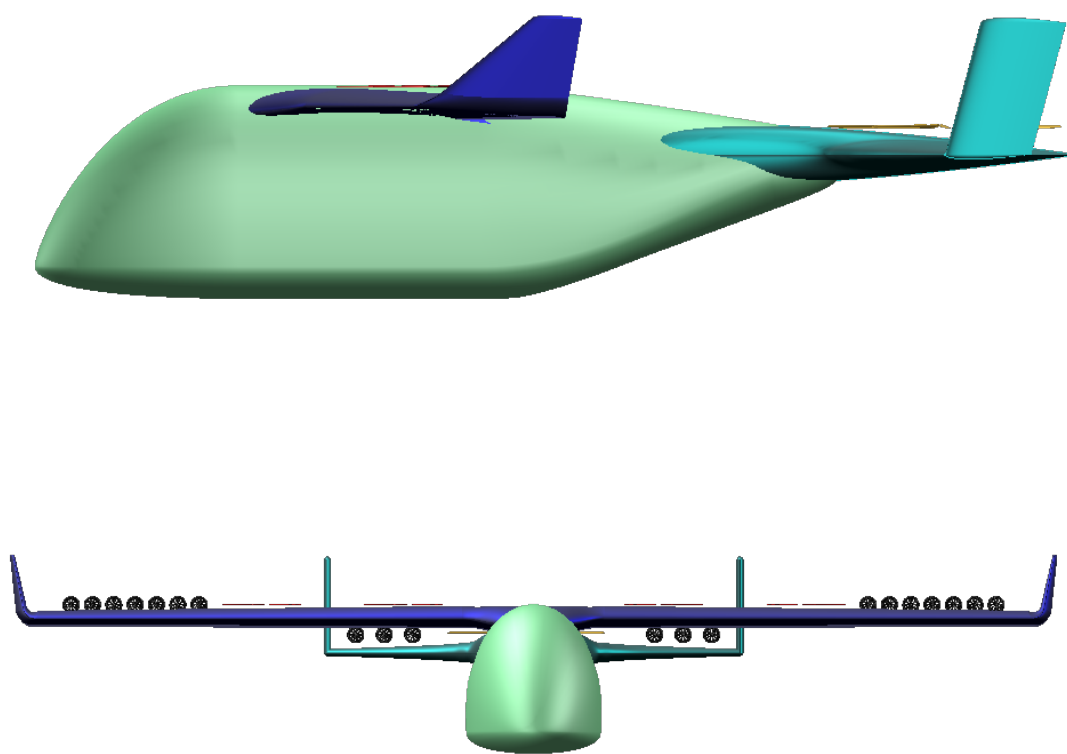


Figure 52: Different views for the final design.

Nevertheless, it is expected that the results are reasonably accurate. This can be justified by looking at the mesh quality as described next.

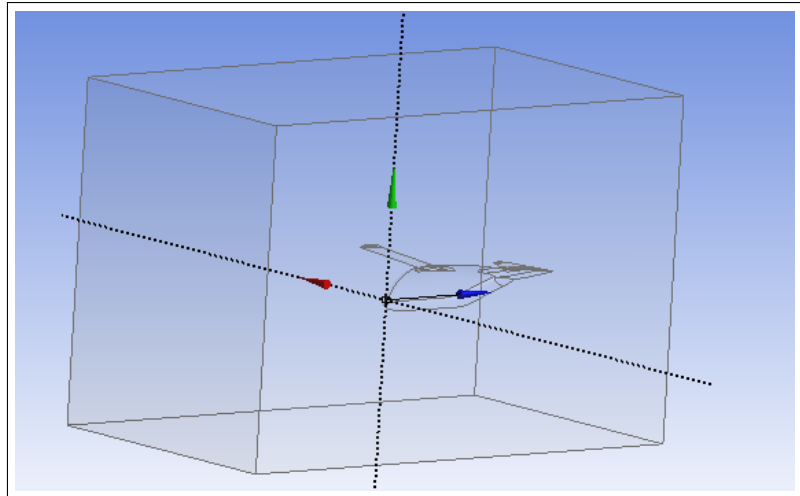


Figure 53: Half geometry as the flow is symmetrical

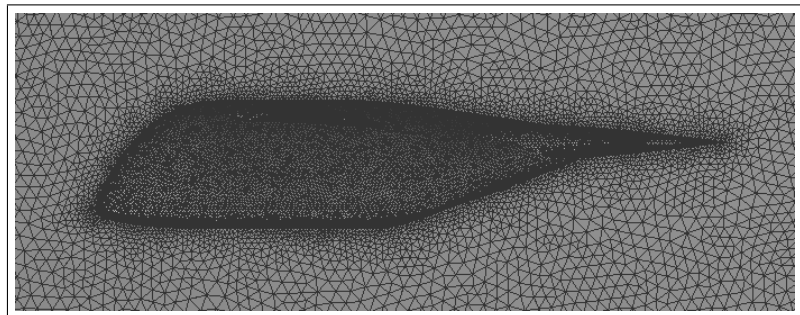


Figure 54: Fuselage Mesh

10.2 Mesh Metrics

Some essential Mesh Metrics that needs to be checked before performing any simulation are Skewness, Orthogonality and Aspect Ratio.

- **Skewness:** Skewness is a value that measures how much a cell is deformed from its ideal counterpart. For instance, the skewness of an irregular triangle is measured as the deviation of its edges from the corresponding edges of an equilateral triangle. A lower skewness value ensures the regularity of cells. For triangular cells, the skewness value is recommended to be placed below 0.85 in ANSYS for minimizing the computational errors. The mesh employed in this simulation has an average of only about 0.25

- **Orthogonal Quality:** It gives a measure of how close are the angles between the adjacent element faces with respect to an optimal angle. A value close to 1 is recommended for accurate results. The average value of the orthogonal quality of the model is about 0.77, which is reasonable for triangular mesh.
- **Aspect Ratio:** Aspect ratio is the measure of the stretching of a cell. It is defined as ratio of the shortest edge to the longest edge of a cell. ANSYS recommends an average value between 1 to 5 for accurate results. The mesh was found to have an average value about 1.85.

10.3 Initial Conditions and Boundary Conditions

The flow conditions for the simulation was set to match the free-stream atmospheric conditions at an altitude of 1 Km. The inlet flow was set at 55.56 m/s which is the cruise speed given in the RFP. Since the R_e is about 5-6 million, the laminar flow can trip to turbulent flow with even slight disturbances. Hence Menter's Shear Stress Transport $k - \omega$ model was used as it also suits well for flows that involve flow separation. This model belongs to the **RANS** or Reynolds Averaged Navier-Stokes family of turbulence models. Ideal compressible gas was used with Sutherland's model to compute the dynamic viscosity. The specific heats were kept constant to reduce the complexities in simulation.

Geometry	Boundary Condition
Inlet	55.56 m/s
Outlet	Free-stream conditions
eVTOL Surface	No slip condition
ZX plane	Symmetric plane

(a)

Mach	0.165
Altitude	1 Km
Temperature	281.65 K
Density	1.112
Dynamic Viscosity	1.7894e-05

(b)

Table 10: Setup for the CFD simulation.

10.4 Convergence Criteria & Stability

The CFL number was automatically adjusted to ensure stability. The ideal convergence criteria is to ensure that the residuals reduce below the order of 10^{-6} . This requires enormous computational cost which is not achievable in a limited time frame. This limitation can be overcome by considering an average approach. The average value of C_D and C_L were calculated over each 100 iterations. Once the average values converged within certain error bounds the simulation was terminated. This error bound was kept about 0.1%. The computational time was about 2 hours to achieve the convergence.

10.5 Results

The flow simulation was performed at various angle of attack to get the variation of lift and drag. As shown in the figure 55 below, the maximum lift to drag ratio is 15 at 0° as calculated in xflr5, C_L is 1.16 which is very close to the $C_{L,cruise} = 1.157$. It can be further seen that C_L is still increasing even after 20° angle of attack! This is due to the very fine streamlining of the fuselage, the wings are already stalled at about 20° as predicted by xflr5, refer figure 22. The separation at the wings was captured in the simulation, but the fuselage continues to provide lift even at higher angle of attacks but this comes at the cost of very high drag.

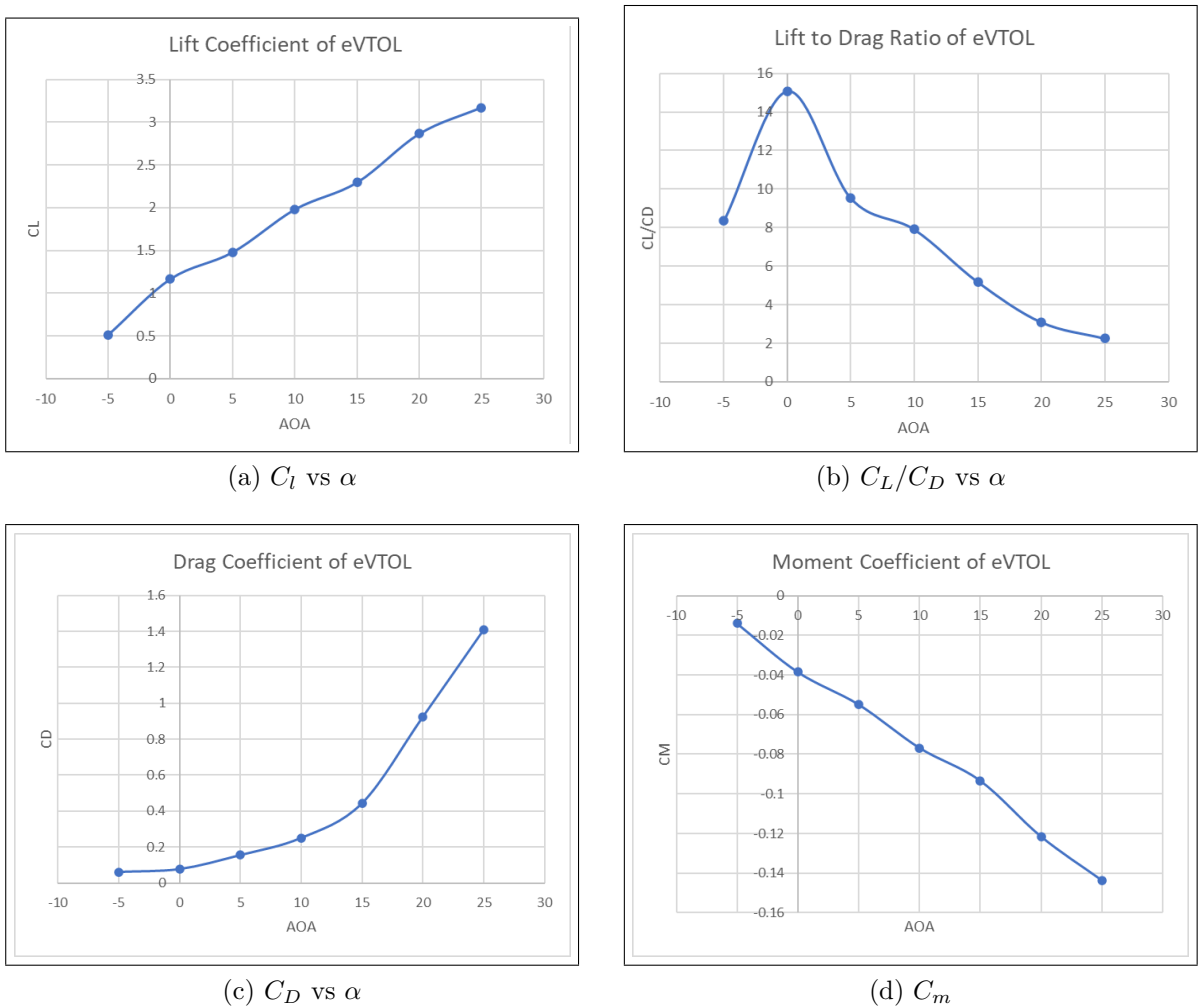


Figure 55: CFD Analysis of the entire eVTOL

11 Mission Profile And Power Requirement

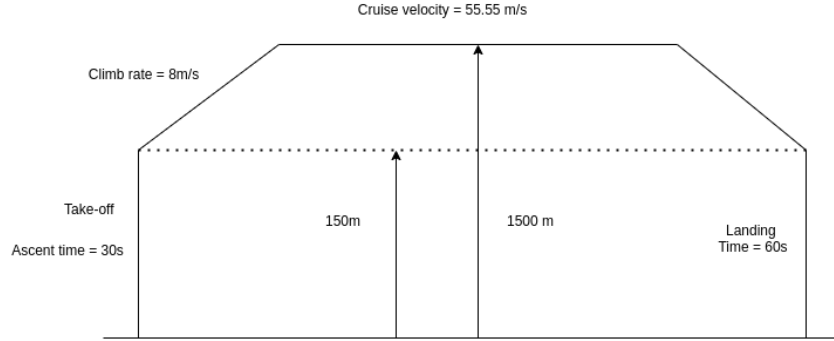


Figure 56: Mission Profile

11.1 Total Energy Required and Endurance

To keep in check that our power source doesn't run out of energy mid flight, we need to carefully carve out a plan so that energy in different stages in the flight plan are utilised properly. A simple way to get a crude estimate for total energy required in the entire mission is noted below :

$$\Sigma [P_{\text{average of each stage}} \times T_{\text{each stage}}] \quad (31)$$

The requirements for solving this problem are the averaged out power required in take off, transition, cruise, loiter or the gliding descent and landing as well as the time in which our eVTOL will be in that particular stage. Once we figure these values out, we will get an estimate of how much total energy we will need to install into the empty weight to execute the mission.

From the blade analysis, the value we get for maximum power required for hovering, is equal to around 1337 kW. At the same time, from sizing estimates, we get the power estimate to be 6.52 times the weight of the eVTOL. Assuming an average flight weight of 3500 kgs, we get the power consumption during cruise flight to be 93.6 kW and at maximum thrust the power required is 312kW. For the entire cruise part of the mission profile, let's consider that our eVTOL is consuming 150 kW at a constant rate for a reality check.

Now that we have values for power required, all we need to do now is to estimate how much time is taken for each stage. We can write down the flight plan as follows on the basis of mission plan stated in section 3 of this report.

Take off and hovering	30 seconds
Transition to Cruise	3 minutes
Cruise Flight	3 hours (max)
Transition to Hover	3 minutes
Hovering and Landing	1 minute

For total power required, let's consider the worst circumstances in our entire mission and to check whether our HyPoint power source can handle it or not. So we will assume that initial 4 minutes consist of our vehicle consuming 1400 kW, consuming 180 kW for cruise flight of 3 hours, and then again consuming 1440 kW for the last phases for 4 minutes. Doing computations for every stage in the mission, we get the total energy required as :

$$\frac{1440 \times 4}{60} + 180 \times 3 + \frac{1440 \times 4}{60} = 732 \text{ kW-hr} \quad (32)$$

Considering the worst possible scenarios of power consumption in our entire mission profile, we still get the value for total power consumption as 732 kW-hr. Now that we have how much energy and power is required to execute the entire mission, let's have a look at how to solve this massive requirements.

12 Propulsive Units and Power Source

12.1 Propulsive Units

In the initial report, we listed mainly two types of Propulsive systems that can potentially work in our eVTOL design. Those are described in short as follows :

1. Electric - Electric Ducted or Unducted Fans or Propellers: (TRL = 9)



Figure 57: Schubeler 195mm EDFs

The EDFs can be independently controlled to deliver thrust in any direction. This technology has been in the market for quite some time now in the aviation industry. The strongest electric ducted fans (EDFs) present in the market right now is the Schuebler 195mm. It produces a thrust of about 250 N, weighs 3.4 kg, has a power consumption of 15.6 kW. The Lilium 2 seater Jet uses 36 EDFs as its only propulsion system. Assuming Lilium uses 36 Schuebler 195mm EDFs, the max thrust possible is 688kgs. The Lilium 2 seater has a maximum takeoff weight of 640 kgs with empty weight equal to 440 kgs. We can clearly see that these EDFs are capable of hovering this jet easily. The drawback of EDFs is its power consumption rate. Those used in Lilium will require a total of 562 kW of power. Even with a Tesla battery pack, which stores 85kWh of energy, can give an endurance of only 9 mins!

2. Ionised Air Plasma Induced by Microwaves/ Electric Plasma Jet Propulsion : (Estimated TRL 3-4)

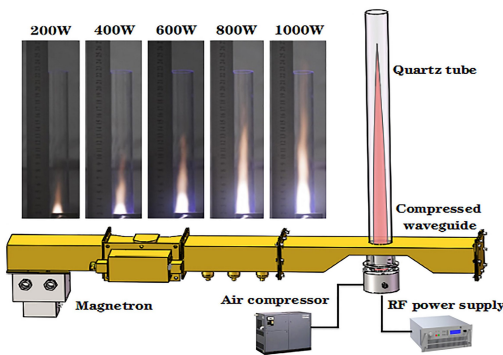


Figure 58: Plasma Jet Propulsion by Wuhan University

Wuhan University constructed a prototype plasma jet device capable of lifting a 1kg steel ball over a 24mm diameter quartz tube. The thrust needed to achieve such lift is equivalent to the relative thrust of a commercial aircraft engine. Pressurized air is injected into a chamber and subjected to over 1,000 degrees Celsius and microwaves to create an ionised plasma, which is then expelled to create propulsion.

From the configuration selection work of ours and due to technological immaturity of Ionised Air Plasma Jet Propulsion, we had to settle for coaxial motors acting as the upward thrust inducing bodies and use electric ducted fans for the forward flight as it was decided the most efficient among all other configurations

in the domain of electric propulsion for the cruise part of the mission profile. However when we are using this many rotors and EDFs, the challenge of using every propulsive unit efficiently comes naturally to us. This seems a really intensive task if you think about the controls system which will be responsible for the operation of the VTOL. But we will assume for now that by 2030, the computational capacity of onboard computers and application regime of controls would be developed to a massive scale to solve this control problem. Hence we can now peacefully go on to decide which power source in the world can possibly satisfy our huge needs for this mission.

12.2 Forward Thrust - EDFs

In this eVTOL, 20 cm diameter EDFs will be used, analogous to Schubeler 195mm. From the ANSYS simulations performed on the entire eVTOL, the drag during the cruise and during stall came out to be roughly 1440 N and 3420 N respectively. Just to be on the safer side, we will consider 5000 N to be our maximum thrust requirement. As thrust produced by one EDF is 250 N, we will be requiring 20 EDFs on the entire eVTOL to achieve that result.

However, we should always remember, we have only considered 5000 N thrust requirement as a safety factor. As redundancy is large in this design, the eVTOL can safely execute its desired plan even if 6 EDFs stop working.

12.3 Key Challenges for Power Source

Usage of a completely green, eco-friendly propulsion source along with the idea to make it last long enough for inter-city travel is a key challenge in this domain. The requirements for our eVTOL demands an extremely powerful and at the same time, durable power source if we compare it to the state of the art technologies. The time when prototypes of Lilium 2-seater Jet are being tested and claimed that it can provide an endurance of about an hour, we would want the endurance to be almost thrice of it and it should carry three more people! Because of this particular deviation from reality, a major challenge in designing the ICeVTOLA is deciding on a power source and making sure that power source is durable enough so that inter city travel objectives doesn't get abandoned midway through flight.

12.4 Approach

We take into consideration the following two specifications of a technology to shortlist our powerhouses and finally make a stand on which power source to use.

- Specific Energy Density which is the gravimetric energy storage density of a battery, expressed in Watt-hours per kilogram (W-hr/kg)
- Specific Power, that is for a battery, it is the gravimetric power density expressed in Watts per kilogram (W/kg)

We obtained a rough estimate of Power required for prototypes made nowadays for eVTOLs which matched our rotor analysis and gave us a range of 1.4MW of maximum Power required for our operation. To achieve this however, we will need the state of the art combined with some futuristic technologies to make the design feasible. Otherwise, almost 50% of the weight of the VTOL would be just filled up with batteries. Which can be firstly, very unreliable from the structural point of view and at that same time, very unsafe if you talk about a transport vehicle. So to figure this out, we researched on upcoming and current technologies that can potentially address this particular issue. The most viable options according to our initial research are as follows :

1. Lithium Ion Battery Technology

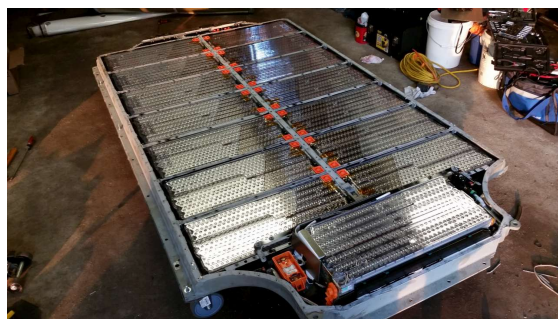


Figure 59: Tesla Model S Battery Pack

If we talk about Li-Ion batteries, Tesla Motors' battery pack for Model S is the pinnacle of it. We will take this battery pack as the reference to this technology and build up our discussion on this. So, according to the design, the battery packs consist of 4,416 lithium ion cells in 2170 cylindrical configuration. The pack has two sets of modules, one set has 23 bricks made up of 46 cells per brick and the other set of modules has 25 bricks made up of 46 cells per brick, producing 350 volts nominally. Tesla Model S battery pack has an energy capacity of 100kWh, max. power of 580kW, battery voltage of 375 V and weighs 625 kg. The drawback is its low energy to weight ratio of 160Wh/kg. Using them in eVTOLs may hinder lift characteristics. But the energy which it stores, and further developments made on the battery pack

from Tesla are promising. Using NMC battery chemistry instead of NCA, can increase the max specific energy from 100Wh/kg to 240Wh/kg.

Although, however cutting edge technology it might be for electric cars as demonstrated by Tesla Motors, we need to understand that this kind of battery source having low energy density values would affect the flying characteristics as its weight would hinder the maneuverability of the eVTOL and at the same time increasing the gross weight, the thrust required to hover and hence the power consumption. Li-Ion batteries specifications can get better through different combinations of battery chemistry, and we hope for that because if these batteries have the potential to power a grid, as demonstrated by Tesla Powercell, it may be very much possible that if research in this domain is accelerated keeping in mind the objective of using this technology in aviation, we will obtain designated battery packs that are specifically designed for eVTOLs.

2. Antora Energy - Heat Battery



Figure 60: Solid State Heat Batteries

It is an example of a solid state battery which is a battery technology that uses solid electrodes and a solid electrolyte, instead of the liquid or polymer gel electrolytes found in lithium-ion or lithium polymer batteries. Materials proposed for use as solid electrolytes in solid-state batteries include ceramics (e.g., oxides, sulfides, phosphates), and solid polymers. Solid-state batteries have found use in pacemakers, RFID and wearable devices. They are potentially safer, with higher energy densities, but at a much higher cost.

Antora Energy is building a low-cost thermal battery for grid-scale energy storage. By combining inexpensive thermal storage media at high temper-

atures with high-efficiency thermo-photo-voltaic energy conversion, it plans to support widespread integration of renewable resources on the electricity grid. Unlike solar energy, this thermal battery will take excess electricity from wind and solar power plants, store it as heat in hot storage medium for hours or days, then some ultra cheap raw materials capture the light radiated from the hot storage medium and convert it back into electricity when needed. This energy storage solution can be used as a secondary source to recharge the main power pack recharging at every moment of action and rest. However promising this technology may look, it is very dicey whether we will be able to witness the implementation in real life application by the year 2030. Hence relying on this technology to just solve all our problems isn't a good idea.

3. Hydrogen Fuel Cells - HyPoint



Figure 61: HyPoint Hydrogen Fuel Cells

The issue of low energy storage capacity can be solved by Hydrogen Fuel Cells. HyPoint, a company, has manufactured air-cooled hydrogen fuel cell power-train that produces 1000 W/kg of specific power with an energy density of 530 Wh/kg which is likely to be far higher than the expected energy density of next decade's lithium-ion batteries with a comparable power output. The company's next version of the product is expected to reach 2,000 W/kg specific power and 960 Wh/kg energy density compared to Tesla's

Battery pack which gives 160 Wh/kg. It is estimated to start production in the next five years. Hydrogen fuel cells can provide improved specific energy over batteries in vehicles that require sustained endurance or range over 100 miles. Fuel cells till date have poor specific power and are not able to provide the power output required by a typical eVTOL aircraft. Hydrogen fuel cells had a vital role in our final selection of the Power Plant option due to its promising energy storage density.

Now considering that ICeVTOLA is aimed to launch into the market by 2030, hydrogen fuel cells have a lot of time to develop. Alakai Skai, is a prototype eVTOL made which is designed to run on hydrogen fuel cells only. HyPoint has stated that the specification of 2000 W/kg specific power and 960 W-hr/kg specific energy density will be achieved by the end of 2023. So if we trust the company to develop this by then, or better, enhance their technology by the year 2030, we will surely get a very good power source to work with. The hassles however, are refueling, storage of liquid hydrogen and other gases, which can go really expensive for initial stages. But if we are talking about 2030, once the arrangements for hydrogen based vehicles and pit stops are all over the country, this entire issue would seem a trifle.

Hence for now, we decided that we will use this particular technology in our VTOL to power our propulsive units, which are rotors and ducted fans purely on hydrogen based fuel cells, very similar to that of Alakai S'kai. To solve the problems of the future, it is evident that we need the tools of the future too. And if we want to enhance our lifestyle, bring this intercity travel in our day to day routine, developments in this domain are very crucial.

12.5 Final Power Source - Weight and Specifications

For further calculations, we are considering HyPoint's Hydrogen Fuel Cells designed for Alakai S'kai which is supposed to come to market by 2023. This technology gives a specific power of 2000 W/kg and a specific energy density of 960 W-hr/kg.

From the sizing part of our work, we can state that the power source weight goes up to 1172 kgs. Multiplying this value of our specific power and specific energy density, we get the absolute maximum available power and maximum energy stored.

Maximum Power Deliverable	2.34 MW
Maximum Energy Stored in the Cell	1125 kW-hr

However, we need to consider the fact that this extrapolation isn't linear and may show some saturated behaviour after a weight limit. Also, we should consider the drop in performance over time and hence for our next considerations we will take only 80% of these values and state that as the specifications of our power source. Hence after considering realistic factors, we get the values as :

Maximum Power Deliverable (Revised)	1.875 MW
Maximum Energy Stored in the Cell (Revised)	900 kW-hr

12.6 Conclusion of Power Calculation

As we found out from the previous subsection of the report, the power requirements for hovering and transition was around 1400 kW or 1.4MW and for the cruise at maximum thrust was 312kW. As maximum power which can be delivered by HyPoint H2 Fuel Cells is 1.875MW, power is not an issue.

Considering the entire mission profile, we require a total energy of 732kW-hr. Our current power source delivers 900kW-hr which leaves us with 18.7% extra energy for emergency conditions. If we assume the mission to be as ideal as possible, 1337kW required at hover, transitions and landing, and 93.6kW for cruising for 3 hours, it leaves us with at least 18 minutes of extra hovering time which can be utilized if there are some difficulties at the helipad. This proves that HyPoint Turbo Air H2 Fuel Cells is a green and viable option to act as a power source for our ICeVTOLA.

Components	Weight in (kg)	X Coordinate (cm)
Wing	750	300
Wing Rotors	142.31	300
EDFs	80	370
Emp Rotor	41.33	900
Empennage	70	880
Power Source / Electronics	1172	423
Fuselage Skin	600	360
Landing Gear	120	360
Pax/Cargo	500	320
Avionics	50	10
Total Gross Weight	3525	CG: 371.95

Table 11: Longitudinal weight distribution

13 Weight Distribution

To assess the stability of an aircraft, one needs to have a breakdown of weight distribution inside the plane. We used several empirical interpolations/extrapolations to calculate the weight of individual parts inside the plane. Table 11 lists down proposed weight distribution along with its longitudinal location. With this distribution, we have the center of gravity at the longitudinal location of 371.95 cm from the plane's nose.

13.1 Wing and EDFs

Wing weight estimate excluding winglets is found out to be 680kg using the material assignment mentioned in Table8. The total wing including winglets weighs around 750kg. Weight estimation for the EDFs was pretty straight forward. The Scheubler 195 weighs around 3.7 kgs. Summing up the installation weight and EDFs weight itself, we can assume each EDF weighs around 4 kgs per piece. We are using 20 EDFs and hence the total weight adds upto 80 kgs.

13.2 Rotors in the Wing and Empennage

The material used for blades is Woven Carbon Epoxy with stainless steel erosion strip at the leading edge of the blade to prevent wear and tear at the leading edge from the high pressure. The Woven Carbon Epoxy has a density about 1750kg/m^3 .

Blade Parameters	Wing Rotor	Empennage Rotor
Radius	0.625 m	1.25 m
Mean chord	0.0625 m	0.1072 m
Thickness	21%	21%
Volume	0.0002645 m^3	0.001508 m^3
Mass	0.463 Kg	2.640 Kg
Total Blades	8 x 10	1 x 10
Total Mass	37.04 Kg	26.40 Kg
Mass fraction of hub & motor combined	0.74	0.37
Total Mass	142.31 Kg	41.33 Kg

Table 12: Rotor weight estimation.

The mass of the motors are calculated using an empirical relation given in [7], refer eqn (33) in SI units, and accordingly their mass fractions are represented in the tabular format above, since the empennage rotor has to spin only half the RPM as that of the wing rotors the electric motor's mass reduces considerably.

$$mass_{motor} = \frac{58}{990}(1.3558 \times \tau - 10) + 2 \quad (33)$$

13.3 Landing Gear and Avionics

Equations based on empirical data for a similar category of planes were used for estimating the weights of landing gear, and avionics [7]. Equation 34 lists the used expressions. GW refers to the gross weight of the aircraft in lb . Weights of landing gear (W_{lg}) and the avionics ($W_{avionics}$) are also in lb . For our usages, values were converted back to the SI units.

For the gross weight of $3527kg$ we get $W_{lg} = 120kg$ and $W_{avionics} = 50kg$.

$$W_{lg} = 40 \left(\frac{GW}{1000} \right)^{0.67} n_{wheels}^{0.54}$$

$$W_{avionics} = 0.0268^{GW} \quad (34)$$

13.4 Miscellaneous Weights

The weight estimation of the Power Source is a crucial part when it comes to longitudinal stability as it weighs almost 1/3rd of the entire eVTOL(1172 kgs). HyPoint Turbo Air Cooled H2 Fuel Cells power source doesn't have a prototype

yet. We can expect one by the end of 2023. Nevertheless, we can assume that the setup's weight can be distributed in different parts of the vehicle. The total weight of the power source was divided into two parts consisting of 40% and 60%. The lighter section is to be placed near the pilot and the heavier section which will contain the liquid hydrogen tanks occupying at least 1.5m^3 , will be placed behind the passenger/cargo space. Hence, by this distribution, it's concentrated x-location comes around 4.23m from the eVTOL's nose.

Once the estimation for all the individual weights is done, 500 kgs of payload is allotted to passengers/cargo weight lying in the designated space. Also, for the structure and skin of fuselage is estimated to be roughly 600 kgs. The x-locations for fuselage's COM and payload are 3.6m and 3.2m from the nose of the eVTOL respectively. We will now use this data of weight distribution for stability analysis in longitudinal and lateral motion in the next section.

14 Performance Analysis

The eVTOL is designed to operate at its highest efficiency at a cruise altitude of 1 Km. It has the longest range at the cruise speed and has enough power to loiter incase of emergency conditions. The EDFs and rotors can be used together in times of emergency if needed. This section deals with the performance analysis of designed eVTOL.

14.1 Range Study

The Brequet's equation for eVTOLs or for any electric aircraft is computed using the formula as mentioned in [6].

$$R = \frac{E^* \eta_{total}}{g} \left(\frac{L}{D} \right)_{max} \left(\frac{m_{battery}}{m_{total}} \right) \frac{1}{g} \quad (35)$$

Replacing m_{total} with $m_{eVTOL} + m_{payload}$ in the above equation we derive

$$R = \frac{E^* \eta_{total}}{g} \left(\frac{L}{D} \right)_{max} \left(\frac{m_{battery}}{m_{eVTOL} + m_{payload}} \right) \frac{1}{g} \quad (36)$$

The above equation is interesting to note that the range is independent of the flight speed, but it has an indirect effect through the lift to drag ratio. To maximize the range we need to maximize one of the following terms:

- $\frac{L}{D}$

- Specific energy capacity E^*
- η_{total}
- the ratio $\frac{m_{battery}}{m_{total}}$

The term $\frac{L}{D}$ is controlled entirely by the design process. Although the limit on this term depends on the class of aircraft, it is possible to design it in a certain way such that for most of the *off-design-conditions* the aircraft still performs close to the ideal cruise conditions. And this is what exactly our eVTOL does. The figure 64 give an insight that a $100Kg$ change in payload affects the change in range by just about $20Km$ irrespective of the altitude at which the aircraft is flying. Even at $\pm 400m$ from the cruise altitude, to travel the same range the tradeoff in payload weight is just about $35Kg$. Or to put in other words the *off-design-conditions* are almost as good as the cruise condition at which the eVTOL performs at the optimum level. The range is maximum at cruise condition of $1Km$ altitude. This is a natural consequence of designing the eVTOL to have the highest lift to drag ratio at cruise conditions.

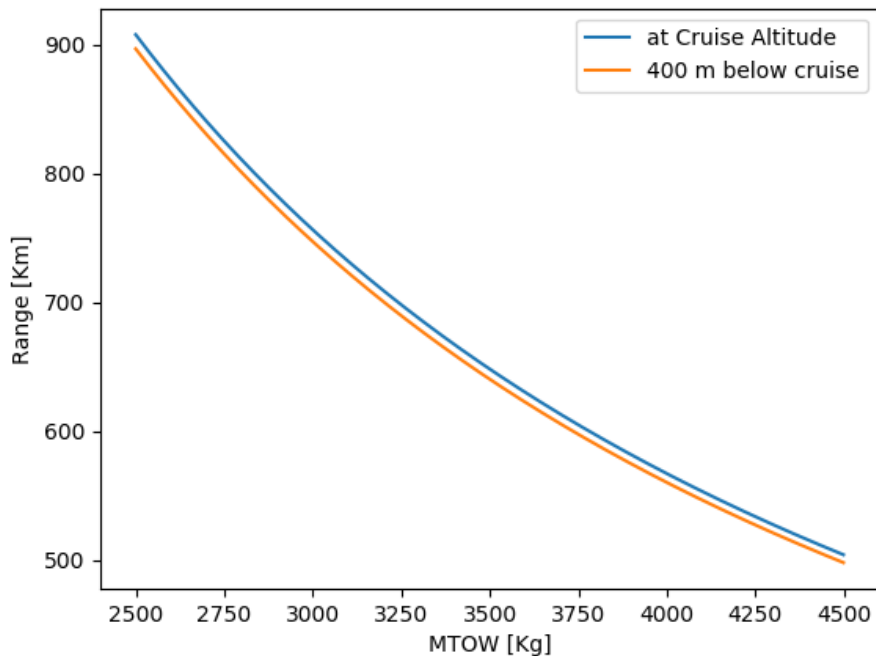


Figure 62: Range vs MTOW

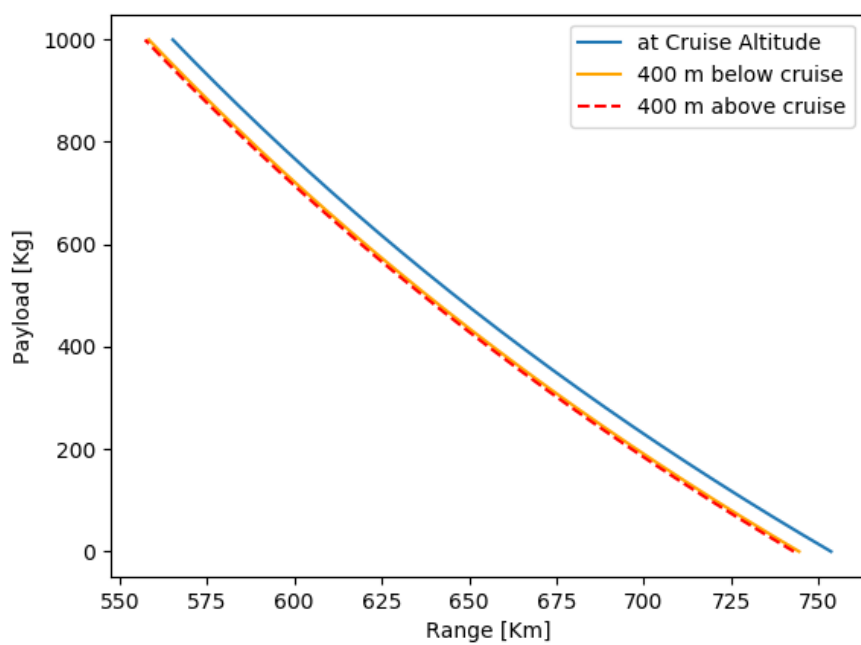


Figure 63: Range vs Payload

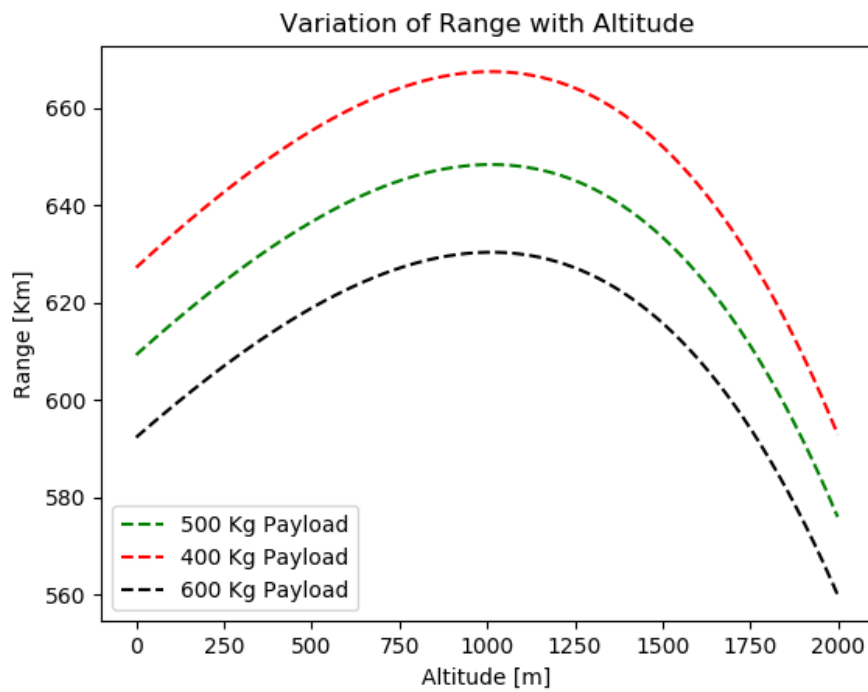


Figure 64: Range vs Altitude

14.2 Forward Flight Analysis

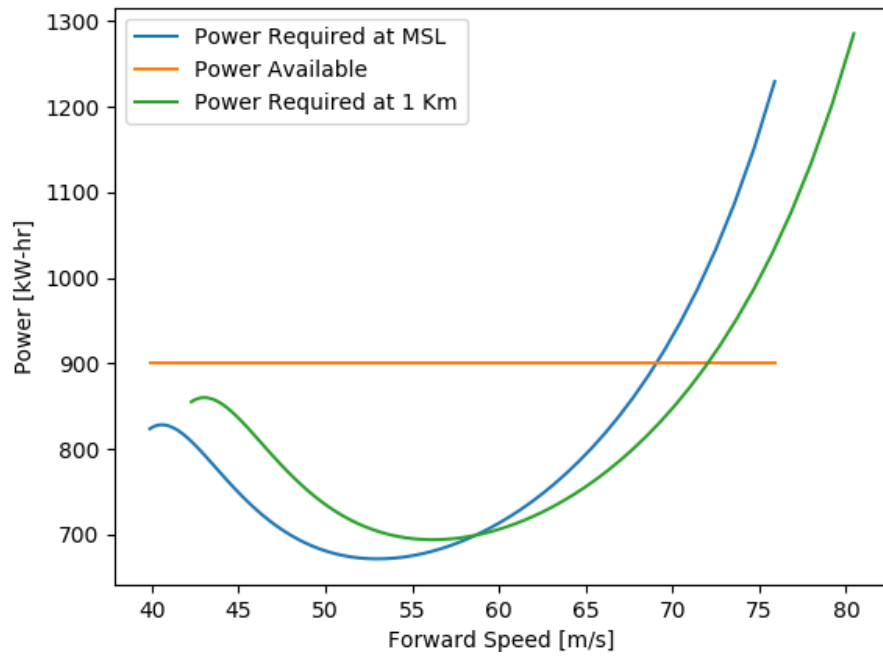


Figure 65: Power vs. Forward speed

The eVTOL is designed to consume the least power at the design cruise speed of 200Km/hr or 55.56m/s . It can be observed from the figure above that the minimum power is intentionally kept close to the cruise speed at different altitudes. The maximum power limits the maximum speed of the aircraft. At MSL the maximum speed is about 68m/s and at cruise altitude it is about 73m/s which is only slightly above the maximum speed of 250Km/hr or 69.45m/s as per the RFP. Here the power required is as per the calculation for cruise condition which is already explained in 12.5.

14.3 V-n Diagram

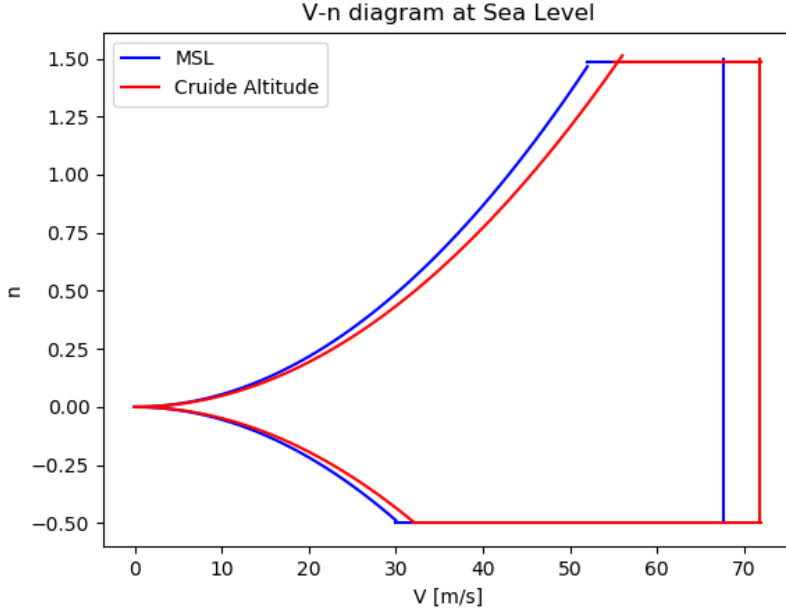


Figure 66: Load factor vs. Speed

Stall occurs when the aircraft is flying at its maximum C_L which is expected to happen in the transition phase near sea level altitude. The wings stall at 20^0 which gives $C_{L,stall}$ as 2.864 from 55. Stall can be calculated as $33.3m/s$. The maximum load factor is $n_{max} = 1.48$ limited by the structural limit at a lift of 52,000 N as explained earlier in wing structural design.

14.4 Sensitivity Analysis

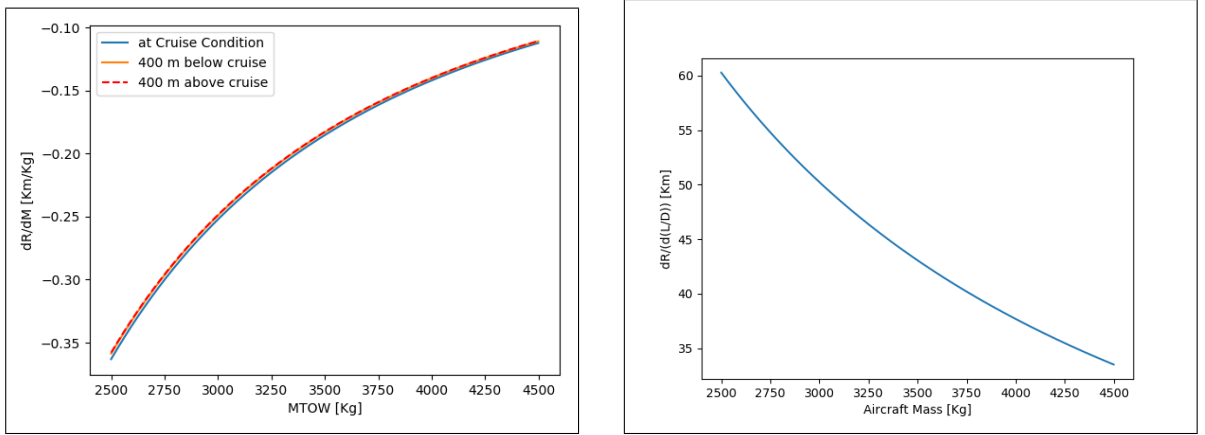
The range equation above can be differentiated with respect to aircraft mass to get the rate of change of range with respect total mass of the aircraft. The figure below 67 gives the inference that a lighter aircraft is more sensible to change in aircraft mass than a heavier eVTOL.

$$\frac{dR}{dm_{total}} = -\frac{E^*\eta_{total}}{g} \left(\frac{L}{D}\right)_{max} \left(\frac{m_{battery}}{m_{total}^2}\right) \frac{1}{g} \quad (37)$$

Similarly

$$\frac{dR}{d(L/D)} = \frac{E^*\eta_{total}}{g} \left(\frac{m_{battery}}{m_{total}^2}\right) \frac{1}{g} \quad (38)$$

The above inference holds true for sensitivity with respect to lift to drag ratio



(a) Range Sensitivity with respect to Aircraft Mass

(b) Range Sensitivity with respect to Lift to Drag Ratio

Figure 67: Range Sensitivity

15 Stability Analysis

15.1 Longitudinal and Lateral Static Stability.

Static stability of the aircraft was analyzed using XFLR5. Through several iterations, weight was distributed along the longitudinal axis such that we have an appropriate static margin. For the weight distribution discussed in table 11, the static margin for the aircraft comes out to be +0.15, which lies in the suggested range for the value in the literature. Simplified model used for the analysis is shown in figure 68. Figure 69 displays the calculated trim condition for the aircraft. Required values for trim fall near the calculated behavior of the aircraft for different angles of attacks. At the trim condition, obtained aerodynamic efficiency is near the maximum efficiency for the plane.

Results for modal response for longitudinal and lateral stability analysis are shown in figures 71 and 70 respectively. Analysis suggests that the aircraft is stable.

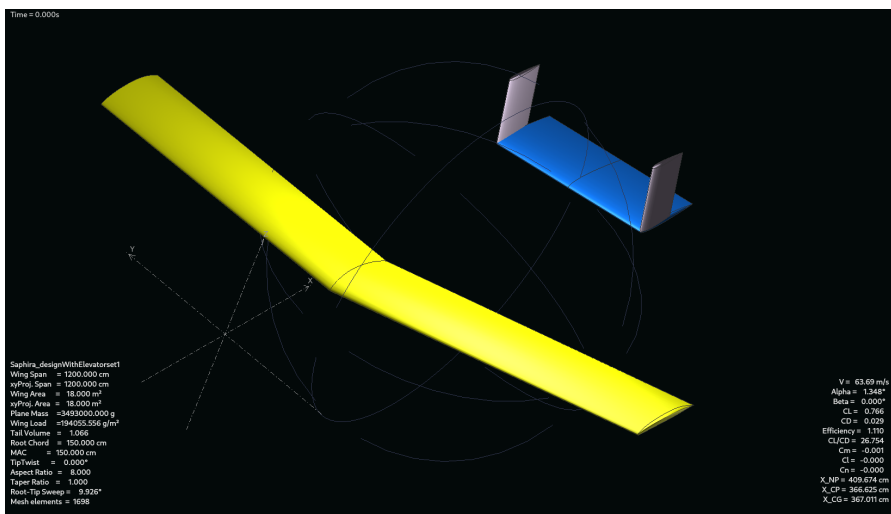


Figure 68: XFLR5 model used for the stability analysis.

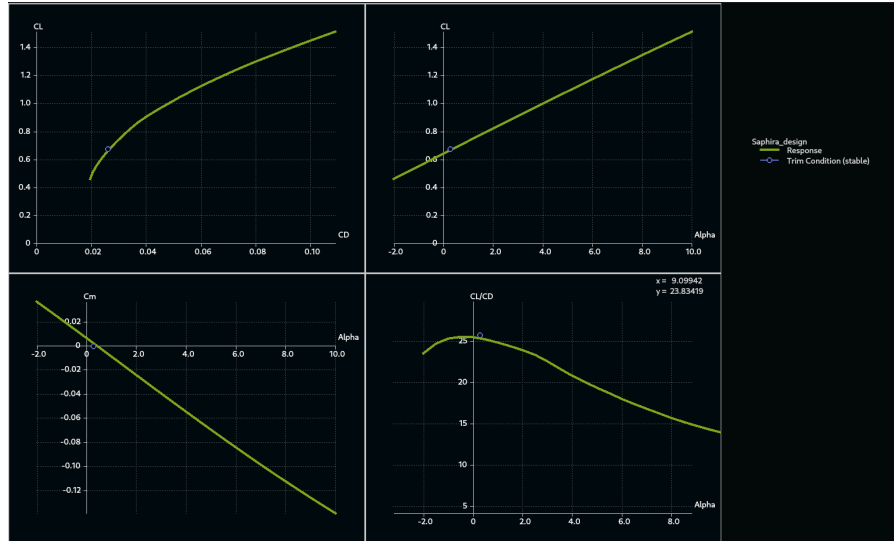
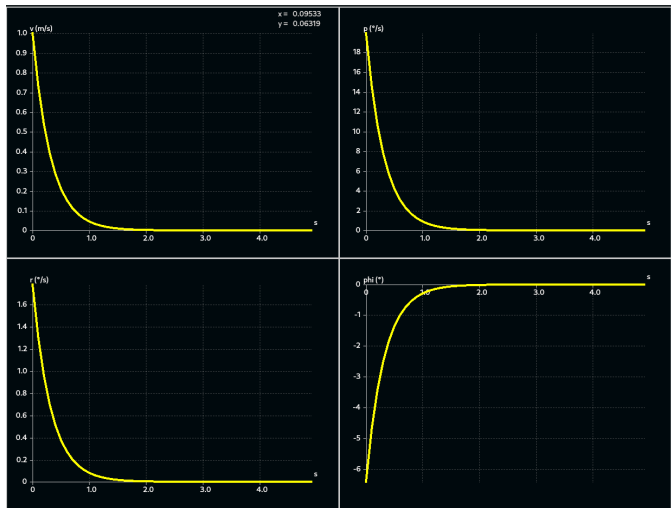
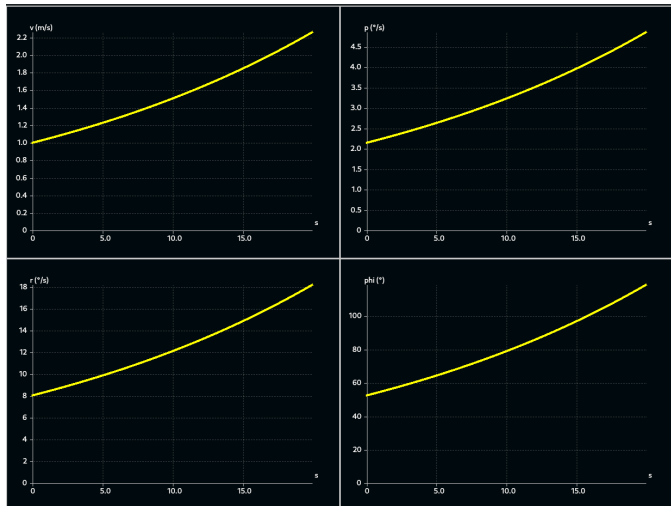


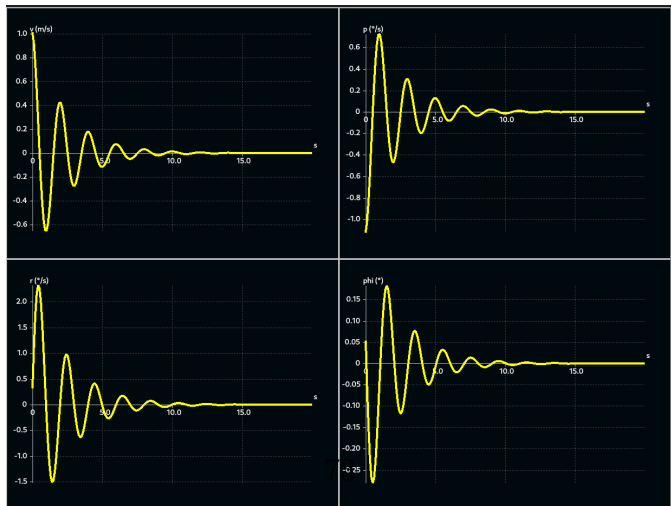
Figure 69: Trim condition for different aerodynamic parameters of the aircraft.



(a) Roll damping

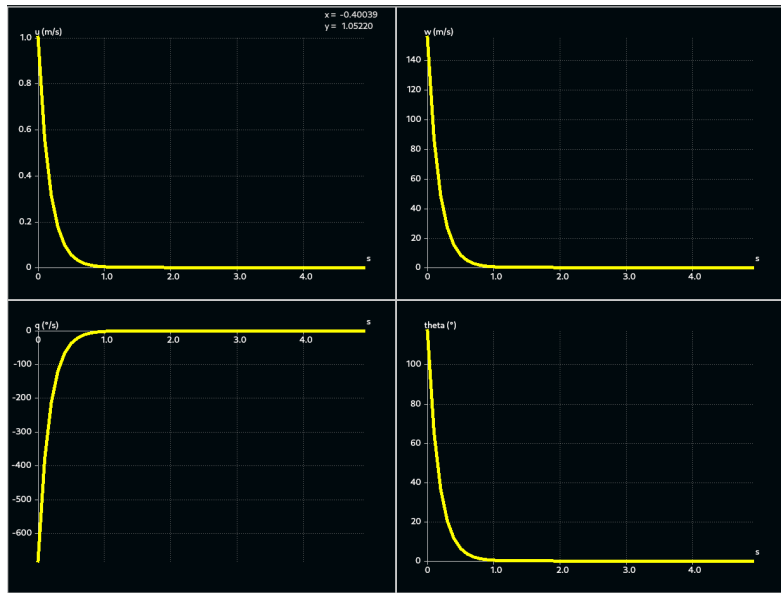


(b) Spiral Mode

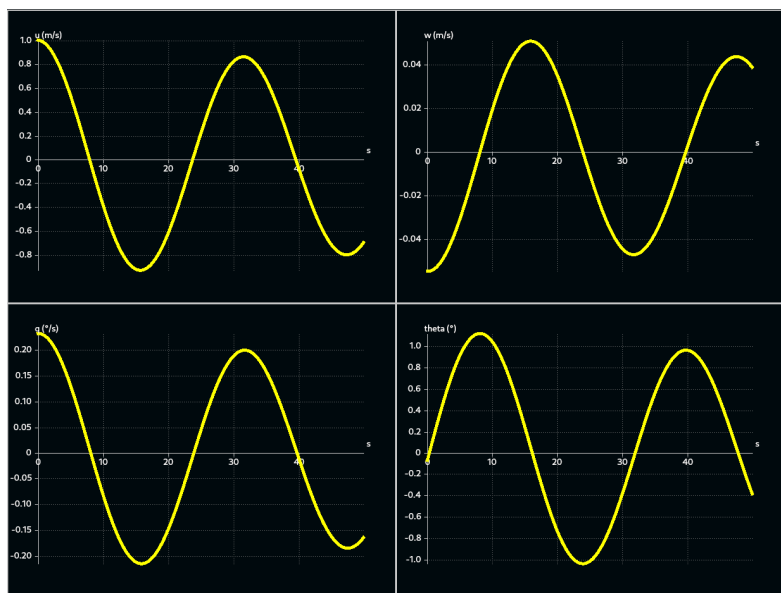


(c) Dutch roll

Figure 70: Modal response for lateral stability.



(a) Short Period Mode



(b) Phugoid Mode

Figure 71: Modal response for longitudinal stability.

16 Acquisition and Operation Cost Estimation

The method used to estimate cost analysis is obtained from [9] which is on the principles of DAPCA-IV method. The latest formulae are available only for 2012 so the final expression for cost was adjusted for inflation. The values are just initial estimates for cost analysis. But before using the formulae directly the quantity of such eVTOLs need to be estimated to come up with a final reasonable cost per eVTOL. As per the study [4] it is expected that worldwide the number of eVTOL will reach about 15,000 in 2035. With an entry in service by 2030, 2000 seems a reasonable quantity to produce. In this cost estimate we consider four primary quantities.

- Engineer hours: includes airframe design, systems engineering, configuration analysis etc.
- Tooling hours: includes design, development, fabrication etc.
- Manufacturing labour: forming, machining, fastening and all manual work
- Quality control: it is a subset of manufacturing but estimated separately. It includes inspection, production inspection and other quality control aspects
- Manufacturing materials: include all the raw material, hardware equipment, prepreg graphite composites etc.

	Man Hours per Unit	Rate for 1 unit[Rs/hr]	Total Cost per unit
Engineering	208	8556	17,79,648
Tooling	265	8780	23,26,700
Manufacturing	3883	8035	3,11,99,905
Quality Control	295	7292	21,51,140
Materials	154952	/	1,54,952
Total (After Adjusting for composites & inflation)			7,04,10,310

$$H_E = 5.18W_e^{0.777}V^{0.894}Q^{0.163} \quad (39)$$

$$H_T = 7.22W_e^{0.777}V^{0.969}Q^{0.263} \quad (40)$$

$$H_M = 7.37W_e^{0.82}V^{0.484}Q^{0.641} \quad (41)$$

$$H_Q = 0.133 \times H_M \quad (42)$$

$$C_M = 31.2W_e^{0.921}V^{0.621}Q^{0.799} \quad (43)$$

The above equations are in USD so they were first adjusted for inflation of 1.17\$ and then converted to rupees as per the current exchange rate. It should also be noted that the labour costs in India could be cheap, this is not accounted in the calculation, but if it is incorporated then it might be possible to decrease the cost further.

16.1 Operating Cost Estimate

The operation cost include

- Energy Costs: Liquid Hydrogen to be refilled at every ride, which is about 96 kgs and requires *Rs.2016* per ride
- Maintenance Costs : This is captured in terms of *Maintenance to Flight Hour Ratio* which is detailed below.
- Inspection cost: Every aircraft requires a certain amount of inspection per year. And this adds to the operation cost.

$$F_{MF} = 0.3 + F_{gear} + F_{fuel} \quad (44)$$

$F_{gear} = 0.02$, $F_{fuel} = 0.01$, their sum F_{MF} being 0.33. The maintenance cost by the mechanic is already included in the below formulae through the term R_{AP}

$$C_{AP} = R_{AP}F_{MF}Q_{FLGT} \quad (45)$$

Where R_{AP} is the hourly rate for a certified Air-frame and Power-plant mechanic (AP) which is about *Rs.3000* per hour. Q_{FLGT} is the number of flight hours per year. We expect a flight hour of 5 hour each day per eVTOL. Inspection costs can be about *Rs.37,500* as mentioned in [4]. Finally, for one year the total maintenance cost is calculated from the above formulae.

$$C_{AP} = \text{Rs.18,06,750}$$

Adding the inspection cost and the total refuelling cost for one year to the total cost, the final operating cost is

$$Cost_{Operating} = \text{Rs.25,42,590}$$

17 Conclusion

Our final design is an eVTOL aircraft with cruise performance much similar to the fixed-wing plane. It employs, Hydrogen fuel cells for generating the propulsive power. Our design satisfies all the requirements described in the NACDEC-IV mission requirements. Starting from the initial weight estimation we carried out initial sizing, then separate detailed designs for rotor blades, wings, fuselage and the tail were carried out. CFD simulations were carried out to calculate the aerodynamic coefficients of the aircraft. Below is a comparison between the mission requirements and status of the eVTOL which are achievable.

Parameter	Requirement	Status
Range	500 Km	645 Km (with 500 Kg payload)
Payload Capacity	500 kg	Additional 500 Kgs of payload for 500 Km range
Air Taxi Mode	4 Pax and $0.5\ m^3$ cargo	Achieved
Air Cargo Mode	$1.5\ m^3$ cargo hold	Re-configurable seats to accommodate payload
Cruise and Maximum speed	200 and 250 kmph TAS	Max. speed 262.8 <i>Km/hr</i>
Powerplant	Green	Achieved with Hydrogen Fuel Cells
Operational Constraints	Takeoff and landing from building rooftop	Achievable
Enroute constraints	Maintain separation of 600 m	Design cruise altitude is 1 km
Entry to market	Before 1 st January 2031	HyPoint plans to develop a prototype by 2023

Table 13: Comparing final design against the requirements.

References

- [1] Alessandro Bacchini and Enrico Cestino. Electric vtol configurations comparison. *Aerospace*, 6(3), 2019.
- [2] Colin P. Coleman. A survey of theoretical and experimental coaxial rotor aerodynamic research. *NASA Technical Paper (3675)*, March 1997.
- [3] Alfred Gessow Rotorcraft Center Department of Aerospace Engineering, University of Maryland. Excalibur. In *Annual AHS International*, 2011.
- [4] Steffan et al. Doppler. In *The future of vertical mobility: Sizing the market for passengers, inspection, and goods services until 2035*. Porsche Consulting, 2018.
- [5] D. Finger, Carsten Braun, and Cees Bil. An initial sizing methodology for hybrid-electric light aircraft. 06 2018.
- [6] M. Hepperle. Electric flight—potential and limitations;. *German Aerospace Center, DLR: Braunschweig*, 2012.
- [7] Akshay R. Kadhiresan and Michael J. Duffy. *Conceptual Design and Mission Analysis for eVTOL Urban Air Mobility Flight Vehicle Configurations*.
- [8] J. Gordon Leishman. *Principles of Helicopter Aerodynamics*. CAMBRIDGE UNIVERSITY PRESS, 2016.
- [9] Daniel P. Raymer. *Aircraft Design - A Conceptual Approach*. AIAA, 2000.
- [10] Metaltail team. In *35th Annual AHS Student Design Competition: A Reconfigurable VTOL Aircraft*, 2017-18.
- [11] Mistral Air Taxi The Huggy's Birds. Electric vertical takeoff and landing (e-vtol) aircraft. In *AIAA GRADUATE TEAM AIRCRAFT DESIGN COMPETITION*, 2018-2019.
- [12] J. Xiao, N. Salk, and K. Haran. Conceptual design of an evtol air shuttle for rapid intercity transport. In *2020 IEEE Power and Energy Conference at Illinois (PECI)*, pages 1–8, 2020.